

OPEN ACCESS

Citation: Biondi G, McCormick G, Fernandez MP (2024) The *Drosophila* circadian clock gene *cycle* controls the development of clock neurons. PLoS Genet 20(10): e1011441. https://doi.org/10.1371/journal.pgen.1011441

Editor: John Ewer, Universidad de Valparaiso,

Received: March 24, 2024

Accepted: September 27, 2024

Published: October 21, 2024

Peer Review History: PLOS recognizes the benefits of transparency in the peer review process; therefore, we enable the publication of all of the content of peer review and author responses alongside final, published articles. The editorial history of this article is available here: https://doi.org/10.1371/journal.pgen.1011441

Copyright: © 2024 Biondi et al. This is an open access article distributed under the terms of the Creative Commons Attribution License, which permits unrestricted use, distribution, and reproduction in any medium, provided the original author and source are credited.

Data Availability Statement: All the data are freely available, without restrictions, and it can be found here: https://github.com/graceb4/cyc-ms-raw-data.

Funding: This work was supported by a National Science Foundation (NSF IOS 2239994) to M.P.F.

RESEARCH ARTICLE

The *Drosophila* circadian clock gene *cycle* controls the development of clock neurons

Grace Biondi¹, Gina McCormick¹, Maria P. Fernandez^{1,2}*

- 1 Department of Neuroscience and Behavior, Barnard College, New York, New York, United States of America, 2 Department of Biology, Indiana University Bloomington, Bloomington, Indiana, United States of America
- * fernanm@iu.edu

Abstract

Daily behavioral and physiological rhythms are controlled by the brain's circadian timekeeping system, a synchronized network of neurons that maintains endogenous molecular oscillations. These oscillations are based on transcriptional feedback loops of clock genes, which in Drosophila include the transcriptional activators Clock (Clk) and cycle (cyc). While the mechanisms underlying this molecular clock are very well characterized, the roles that the core clock genes play in neuronal physiology and development are much less understood. The *Drosophila* timekeeping center is composed of ~150 clock neurons, among which the four small ventral lateral neurons (sLN_vs) are the most dominant pacemakers under constant conditions. Here, we show that downregulating the clock gene cyc specifically in the Pdf-expressing neurons leads to decreased fasciculation both in larval and adult brains. This effect is due to a developmental role of cyc, as both knocking down cyc or expressing a dominant negative form of cyc exclusively during development lead to defasciculation phenotypes in adult clock neurons. Clk downregulation also leads to developmental effects on sLNv morphology. Our results reveal a non-circadian role for cyc, shedding light on the additional functions of circadian clock genes in the development of the nervous system.

Author summary

Daily behaviors and physiological processes are governed by the brain's circadian clock, a network of neurons that regulates internal rhythms through cyclic gene expression. In *Drosophila* (fruit flies), the circadian clock consists of approximately 150 neurons, with a small subset playing a key role in maintaining these rhythms. While the molecular mechanisms of clock genes, including *Clock* (Clk) and *cycle* (cyc), are well understood in terms of timekeeping, their roles in other aspects of neuronal physiology are less explored. In this study, we found that the *cyc* gene, beyond its function in maintaining circadian rhythms, also influences the development of key clock neurons. Specifically, reducing *cyc* expression in a group of clock neurons during development leads to defects in the morphology of those neurons in both larval and adult stages and affects the ability of adult flies to maintain behavioral rhythms in the absence of environmental cues. These findings

This grant provided the salary for G.B. The funders had no role in study design, data collection and analysis, decision to publish, or preparation of the manuscript.

Competing interests: The authors have declared that no competing interests exist.

reveal that clock genes like *cyc* have important roles in brain development, highlighting their broader significance beyond circadian regulation. This work provides new insights into how genetic factors involved in timekeeping also contribute to the formation of neural circuits, expanding our understanding of the diverse functions of circadian clock genes.

Introduction

The proper wiring of neuronal circuits during development is essential for the neuronal control of behavior. Across animal species, sleep/wake cycle rhythms, as well as many other behavioral and physiological rhythms, are controlled by the circadian timekeeping system, a network of neurons that maintains endogenous molecular oscillations and rhythmic behavior with a ~24 hour period [1]. The proper functioning of this circadian network requires the formation of synaptic and peptidergic connections during development [2,3].

The *Drosophila* circadian clock neuron network comprises ~150 neurons and is the functional equivalent of the mammalian suprachiasmatic nuclei, which contain 20,000 neurons in mice [4–6]. All circadian clock neurons contain an intracellular molecular clock consisting of a transcriptional feedback loop of clock genes[7]. CLOCK (CLK) and CYCLE (CYC) are heterodimeric transcriptional activators that directly activate transcription of the *period* (*per*) and *timeless* (*tim*) genes. PER and TIM encode repressors that inhibit CLK-CYC function. Subsequently, PER and TIM are degraded, which enables the cycle to reinitiate every morning. CLK and CYC also interact with other genes in a secondary circadian loop by activating the genes *vrille* (*vri*), and *Par domain proteine* (*Pdp1e*) [8, 9]. *Clk* and *cyc* expression can be detected in almost all clock neurons even before some of these neurons show molecular oscillations [10], suggesting that these genes serve functions that precede the establishment of molecular rhythms.

Drosophila clock neurons are classified into multiple clusters with distinct patterns of gene expression, anatomy, physiology, and synaptic connectivity [5, 6, 11–16]. Among these clusters, the small ventral lateral neurons ($\rm sLN_v s$) are considered the most dominant pacemakers since they are critical for maintaining behavioral rhythmicity under constant darkness and temperature (DD, or free-running) [17–20]. The $\rm sLN_v s$ release the neuropeptide Pigment Dispersing Factor (PDF) [21], a key output signal within the clock neuron network [22]. PDF accumulates rhythmically at the $\rm sLN_v$ dorsal termini [23] and can be released from both the neurites and soma [24]. Loss of PDF severely reduces the amplitude of the endogenous circadian rhythm and shortens its free-running period in DD [21]. The large $\rm LN_v s$ also produce PDF but do not play a role in maintaining rhythms in DD [17].

The projections of the four $\rm sLN_v s$ form a bundle and remain fasciculated as they extend from the ventral to the dorsal brain during development. These four projections are usually difficult to distinguish from each other until they begin to defasciculate in the dorsal protocerebrum [25] and extend their dorsal arborizations toward the area where dorsal clusters of clock neurons are located [26]. In adult flies, the dorsal termini of the $\rm sLN_v$ projections show rhythmic structural plasticity [27], which relies on daily and circadian rhythms in outgrowth and fasciculation [28–31]. Both $\it Clk$ and $\it cyc$ mutants have lower $\it Pdf$ RNA levels, and the PDF peptide can barely be detected in the $\it sLNv$ projections [23, 32].

Cyc is a homolog of the mammalian gene *Bmal1*, although CYC protein levels do not cycle, unlike BMAL1 and several other *Drosophila* circadian proteins [33]. There is growing evidence for non-circadian functions of BMAL1. First, its downregulation induces apoptosis and cell-

cycle arrest in Glioblastoma Stem Cells (GSC), and it was found to preferentially bind metabolic genes and associate with active chromatin regions in GSCs [34]. Second, brain knockdown of *Bmal1* using CRISPR/Cas9 made glioblastomas grow at faster rates than controls [35], and similar effects were observed in B16 melanoma cells. Moreover, *Bmal1*(-/-) mice exhibit defects in short- and long-term memory formation [36] and show reduced lifespan and multiple symptoms of premature aging [37]. Overall, results from studies in different animal models suggest that *Bmal1* plays a role in the development of various neurological disorders [38].

The *Drosophila* sLN_vs offer an excellent model for exploring the non-circadian roles of canonical clock genes such as *cycle*. To determine if the phenotypes previously observed for *cyc* mutants are specific to PDF expression or involved a broader, non-circadian effect in the development of PDF- expressing cells, we downregulated *cyc* specifically in the *Pdf*-expressing cells and observed pronounced defasciculation of the sLN_v projections. Similar phenotypes were observed upon expression of a dominant negative form of *cyc*. Moreover, we found that *cyc* downregulation in *Pdf*+ cells during development is sufficient to prevent the fasciculation of the adult sLN_vs and results in the loss of behavioral rhythms in adult flies. Manipulations of *Clk* expression also affect sLNv morphology, although remarkably, the phenotypes of *Clk* and *cyc* manipulation differ. Our results show that *cyc* plays a role in the development of pacemaker neurons, which is likely independent of its role in the circadian molecular oscillator.

Results

cyc downregulation in circadian pacemaker neurons affects the formation of sLN_v axon bundles

Mutations in both Clk and cyc severely reduce pdf RNA and neuropeptide levels [23, 32]. In cyc null mutants, sLN_vs projections are often undetectable in larval and adult brains stained with PDF antibodies [23, 39, 40], although around half of the brains show 'stunted' projections [40]. We observed that cyc null mutants (cyc^{01}) showed a substantial reduction in PDF levels at ZT2, consistent with previous studies, but we also noticed the presence of thin, misrouted sLN_v projections in cyc^{01} flies at higher magnification and intensity (S1A Fig). Upon close observation, PDF could often be detected in the sLN_v projections. However, these projections did not form the stereotypical bundle observed in control brains when extending from the anterior medulla toward the dorsal area of the brain.

Because highly defasciculated projections might contribute to the weaker PDF levels observed in cyc^{01} mutants, we examined the structure of the sLN_v projections using a Pdf-RFP transgene, in which a cytosolic Red Fluorescent Protein (RFP) is controlled by the Pdf regulatory sequence [41]. Flies were raised at 28°C throughout development, and experiments were conducted at 28°C in 6–8-day old flies (Fig 1A). In control brains, the projections from the four sLN_vs remain fasciculated, forming a bundle until reaching the superior medial protocerebrum (SMP). In contrast, the sLN_vs of cyc^{01} mutants often began to defasciculate in the ventral brain, near their cell bodies (Fig 1B). Some sLN_v projections were severely misrouted and did not reach the dorsal brain, extending instead toward the midline or other brain regions. As a result, it was possible to distinguish individual projections from each sLN_v even in the ventral brain in most cyc^{01} mutant brains. This is almost never observed in control brains until the sLNv projections reach the main branching point in the SMP. The morphological phenotypes of cyc^{01} flies are highly variable, and in some instances the projections are barely visible (S1B Fig).

To test whether the effect of cyc loss on the LN_vs is cell-autonomous, we next expressed a UAS-cyc dsRNA transgene (UAS-cyc^{RNAi}) using the *Pdf-Gal4* driver. We quantified the length

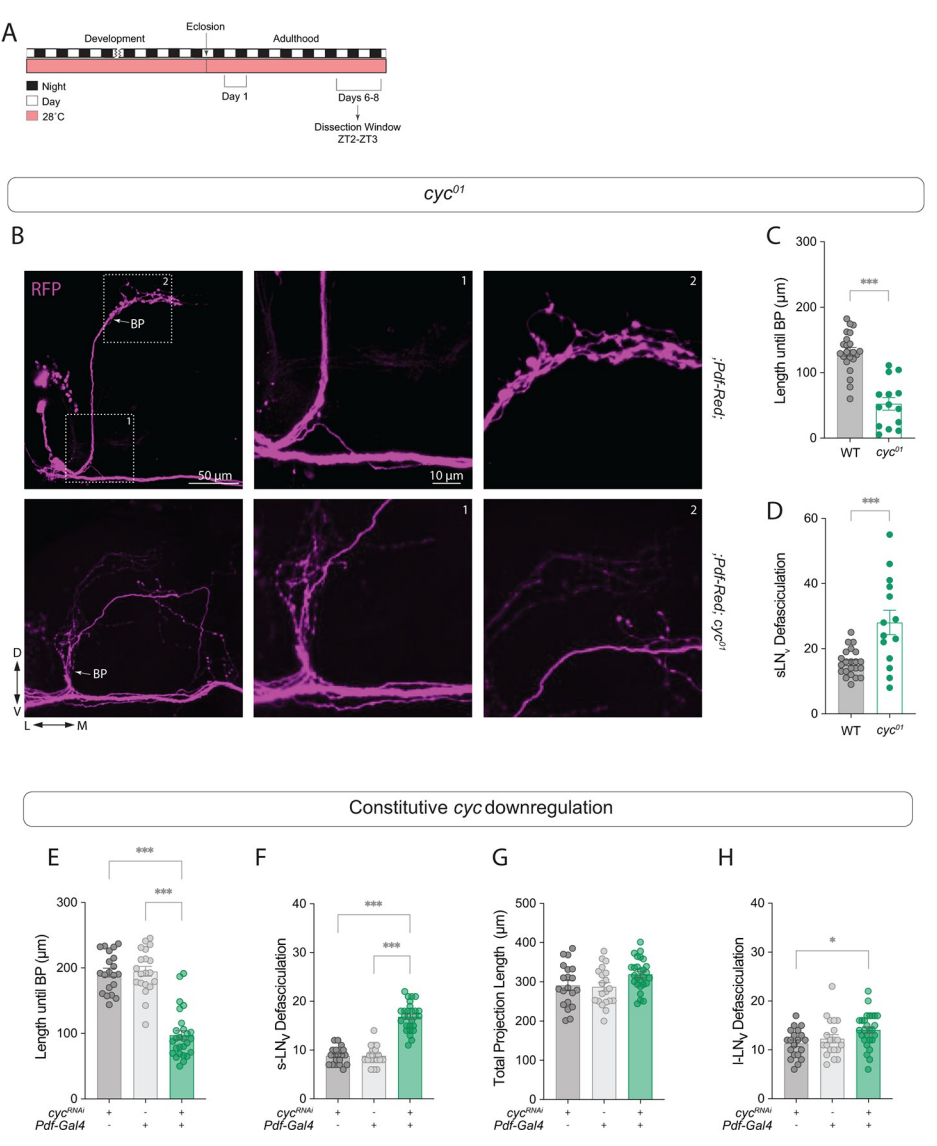


Fig 1. Cyc downregulation in circadian pacemaker neurons prevents the formation of sLN_vs axon bundles. The cyc⁰¹ mutant has disrupted sLN_v morphology. (A) Representative timeline of the experiments in the figure. Flies were kept at 28°C throughout development and experiments were performed within days 6-8 post-eclosion. (B) Representative confocal images of Pdf-RFP controls and; Pdf-RFP;cyc⁰¹ experimental flies stained with anti-RFP (magenta). The branching point (BP) of the dorsal projections is indicated. Scale bar = 25 µm. Boxes with dashed lines indicate the proximal (1) and distal (2) projections, corresponding to the labeled projection images in the center and right panels, respectively. An unpaired t-test was used to quantify the $\mathrm{sLN_v}$ projection length until the branching point (BP) (C), and the total number of intersections of the sLN_v ventral projections (D). Results from two independent experiments, with each dot representing one brain. For each genotype, the number of subjects (n) fall in the range: $13 \leq n \leq 22. \ (\text{E-H}) \ Quantification \ of \ the \ LN_v \ morphology \ phenotypes \ of \ experimental \ flies \ in \ which \ a \ \textit{cyc}^{RNAi}$ transgene was driven by a; Pdf-RFP, Pdf-Gal4; Tub- $Gal80^{ts}$ driver compared to the parental controls. The sLN_v projection length until the branching point (BP) (E), the total number of intersections of the sLN_v ventral projections (F), the total sLN_v projection length (G), and the total number of intersections of the lLN_v projections along the optic tract (OT) (H) are shown. Results from three independent experiments, with each dot representing one brain. For each genotype, the n falls in the range: $20 \le n \le 27$. For nonparametric data sets, statistical comparisons were done with Kruskal-Wallis tests followed by Dunn's multiple comparisons tests. For parametric data sets, statistical comparisons were done with one-way ANOVAs followed by Tukey post hoc tests. Differences that are not significant are not indicated. *p < 0.05, *** p < 0.001. Error bars indicate SEM.

of the projections, starting at the point where the projections of the sLN_vs intersect with those of the lLN_vs ("point of origin", POI, S1C Fig), until the first branching point ("branching point", BP). This branching point is where the sLN_vs ramify and extend their stereotypical arborizations in the dorsal protocerebrum in control brains, and these arborizations show daily, clock-controlled rhythms in their fasciculation and outgrowth [27]. Downregulating cyc in the Pdf-expressing cells significantly decreased the distance to the branching point (Fig 1E). Using a modified Scholl's analysis [42], we quantified the degree of branching in the ventral projections starting at the POI. We observed pronounced defasciculation in the sLN_v projections in $Pdf > cyc^{RNAi}$ flies (Fig 1F). cyc^{01} mutants also showed decreased distance to BP and sLN_v fasciculation (Fig 1C and 1D). The total projection length in $Pdf > cyc^{RNAi}$ flies was not different from that of the controls (Fig 1G), and the defasciculation phenotype was not observed in the contralateral projections that extended from the lLN_vs (Fig 1H). Since the ILN_vs are born later in development during metamorphosis [25], this result suggests that cyc plays a role in neuronal development during an earlier developmental stage, when the sLN_vs begin to extend their projections toward the dorsal brain. These experiments were conducted at 28°C to allow subsequent comparisons with adult-specific and development-specific downregulations of cyc using Gal80^{ts}. Similar results were obtained with flies raised at 25°C (S1F-S1I Fig).

Expression of dominant negative forms of Clk and cyc is an effective strategy for preventing circadian molecular oscillations in specific groups of clock neurons [43–45]. In these dominant negative forms, the DNA binding ability is disrupted while the ability to heterodimerize is preserved [43]. Based on the phenotypes induced by cyc downregulation, we asked if expressing a dominant negative form of cyc in the sLN_vs also leads to aberrant projection morphology. We found that sLN_vs expressing Δ -cyc using Pdf-Gal4 had a significantly shorter distance until the branching point (S2B and S2C Fig) and a greater degree of sLNv projection defasciculation (S2B and S2D Fig), similar to the effects observed in Pdf > cyc^{RNAi} flies. The total projection length and the projections of the lLNvs were unaffected (S2E and S2F Fig).

PER levels in *Pdf*+ neurons are reduced upon cell-specific *cyc* knockdown

CYC activates *per* transcription, and thus, PER levels in the brain are significantly reduced in *cyc* mutants [33]. To test whether the phenotypes of cyc^{RNAi} expression in the Pdf-expressing neurons are consistent with what would be expected from cyc downregulation, we compared PER levels in the parental control (Pdf-Gal4, Pdf-RFP/+) with those in $Pdf > cyc^{RNAi}$ flies at the end of the night (ZT23), when PER nuclear levels are highest [46]. We found that nuclear PER levels in $Pdf > cyc^{RNAi}$ flies were significantly reduced in the sLN_vs (Fig 2B and 2C) and lLN_vs (Fig 2D and 2E). In contrast, PER levels were unaffected in the Dorsal Lateral Neurons (LN_ds) (Fig 2E and 2G). These results confirmed that, at least in a light-dark cycle (LD), $Pdf > cyc^{RNAi}$ flies have lower PER levels in Pdf^+ neurons.

cyc null mutant flies have pronounced behavioral phenotypes. Their activity is unimodal instead of bimodal during LD, and they are predominantly nocturnal [47]. Additionally, cyc mutants are largely arrhythmic in DD due to the key role of cyc in circadian molecular oscillations [33]. We conducted behavioral experiments to determine the extent to which down-regulating cyc specifically in PDF-expressing neurons recapitulates the phenotype of the cyc mutant. We found that at 28°C, the activity pattern of $Pdf > cyc^{RNAi}$ flies was still bimodal in LD (Fig 2H and 2I). However, the majority (~90%) of the experimental flies were arrhythmic in DD (Fig 2J). $Pdf > \Delta$ -cyc flies showed similar behavioral phenotypes (\$2G and \$2H Fig), consistent with what was reported for their free-running behavior at 25°C [43].

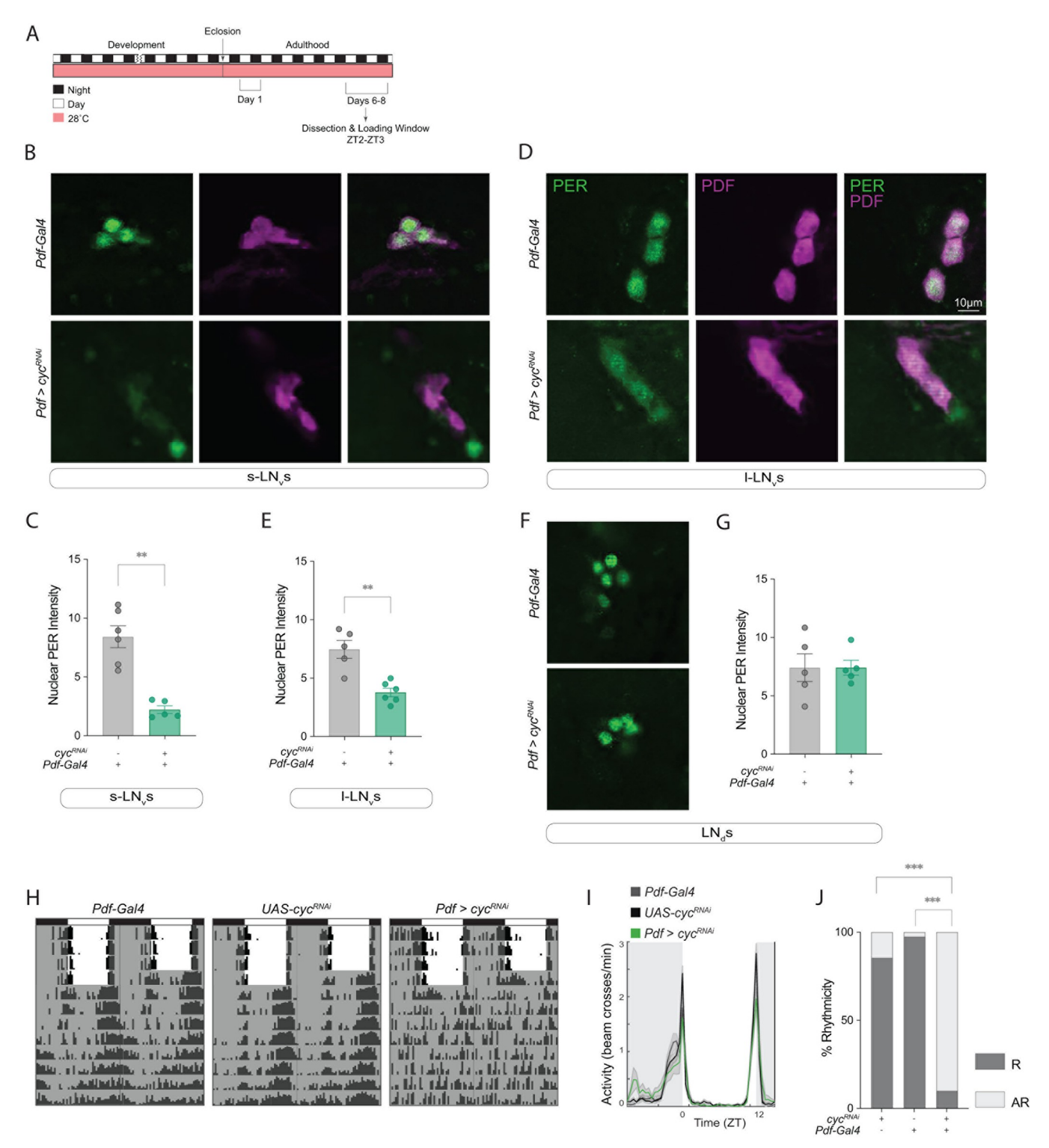


Fig 2. Constitutive cyc downregulation in Pdf+ cells leads to a reduction in PER levels and arrhythmicity under free-running conditions. (A) Representative timeline of the experiments in the figure. Flies were kept at 28° C for their entire lifespan. Experiments were performed within days 6-8 posteclosion. Dissections were performed at ZT2-3. (B,D,F) Representative confocal images of PER (green) and PDF (magenta) staining in the $sLN_{v}s$ (B), $lLN_{v}s$ (D), and $LN_{d}s$ (F) of $Pdf > cyc^{RNAi}$ experimental and Pdf-Gal4/+ control flies (n = 5-6 brains per clock neuron group). All lines also included a Pdf-RFP transgene. Scale bar = $10 \, \mu m$. (C,E,G) Mann-Whitney tests were used to compare nuclear PER intensity levels in the $sLN_{v}s$ (C), $lLN_{v}s$ (E), and $LN_{d}s$ (G) in flies of the indicated genotypes. Differences that are not significant are not indicated. ** p < 0.01. Error bars indicate SEM. (H) Representative actograms of flies of the indicated genotypes under 5 days of LD entrainment followed by 7 days of free-running (DD). To allow comparison with development-specific cyc

downregulation, flies in this experiment were raised at 28° C for their entire lifespan and the experiment was conducted at 28° C. (I) Population activity plots for flies during days 3–5 of the LD cycle at 28° C. (J) Fisher's exact contingency tests were used to analyze the percentage of rhythmic flies of the indicated genotypes under DD (DD1-7). The driver line also included a *tub-Gal80^{ts}* transgene. Additional quantifications can be found in Table 1. R = Rhythmic and AR = arrhythmic. Differences that are not significant are not indicated. *** p < 0.001. Behavioral data corresponds to two independent behavior experiments. For each genotype: $40 \le n \le 48$.

https://doi.org/10.1371/journal.pgen.1011441.g002

cyc acts during development to shape neuronal morphology in adults

To knock down *cyc* specifically during development, we employed a temperature-sensitive Gal80 (Gal80^{ts}) variant with ubiquitous expression to conditionally inhibit Gal4-mediated expression of the RNAi [48]. This method enables the temporal regulation of UAS transgenes, as Gal80^{ts} remains active at lower temperatures but becomes inactive at higher temperatures. We raised flies at 28°C to allow *cyc* downregulation during development then transferred them to 18°C immediately after eclosion (Fig 3A). After 1 week at 18°C, the brains were dissected at ZT2 and stained with PDF and RFP antibodies (see methods section). As shown in Fig 3, downregulating *cyc* exclusively before eclosion resulted in abnormal morphology of the sLN_v axonal projections in adult flies (Fig 3B). The phenotypes resembled those observed with constitutive downregulation, with a significantly shorter distance to the branching point (Fig 3B and 3C) and a greater degree of defasciculation compared to parental controls (Fig 3B–3D). No significant differences were found in the total projection length or the degree of defasciculation of the lLN_vs (Fig 3E and 3F).

A previous study showed that panneuronal rescue of cyc expression in a cyc^{01} mutant exclusively during development was sufficient to partially rescue arrhythmicity in adult flies [40]. Therefore, we asked if downregulating cyc in the Pdf+ cells specifically during development would lead to behavioral phenotypes similar to those seen in the cyc null mutants. We found that under free-running conditions at 18°C, most (~78%) of the $Pdf>cyc^{RNAi}$ flies were arrhythmic (Fig 3G–3I). An analysis of PER subcellular localization in DD2 revealed clear cycling with nuclear PER higher at CT2 (Fig 3J). These results indicate that developmental downregulation of cyc specifically in the Pdf+ cells is sufficient to prevent behavioral rhythms in adults.

To determine whether adult-specific *cyc* knockdown in the *Pdf*-expressing cells would also lead to morphological phenotypes, we raised flies at 18°C and switched them to 28°C immediately after eclosion (S3A Fig, see the methods section). This manipulation did not result in morphological phenotypes either in terms of the length to the branching point or in the degree of sLN_v defasciculation (S3B–S3F Fig). Under free-running 28°C, the majority of the experimental flies were arrhythmic (S3G–S3H Fig), indicating that, as expected, *cyc* is required in adult clock neurons for proper circadian clock function.

Cyc manipulations lead to aberrant sLN_v projections in larval clock neurons

Next, we asked if cyc downregulation results in clock neuron morphology phenotypes during earlier developmental stages. The four larval sLNvs, which modulate the sensitivity of larvae to light and mediate a circadian rhythm in visual sensitivity [49], appear to be identical in their anatomy and synaptic connections [50]. We expressed the cyc^{RNAi} transgene under the Pdf-Gal4 driver and dissected third larval instar (L3) brains (Fig 4). In brains of experimental larvae the length to the branching point did not differ from that of the controls (Fig 4B and 4C), but the degree of dorsal termini branching was significantly higher (Fig 4B-4D). This quantification is similar to that previously described when quantifying the arborization of the dorsal projections sLN_v s in adults [27], where the concentric circles are centered at the main dorsal

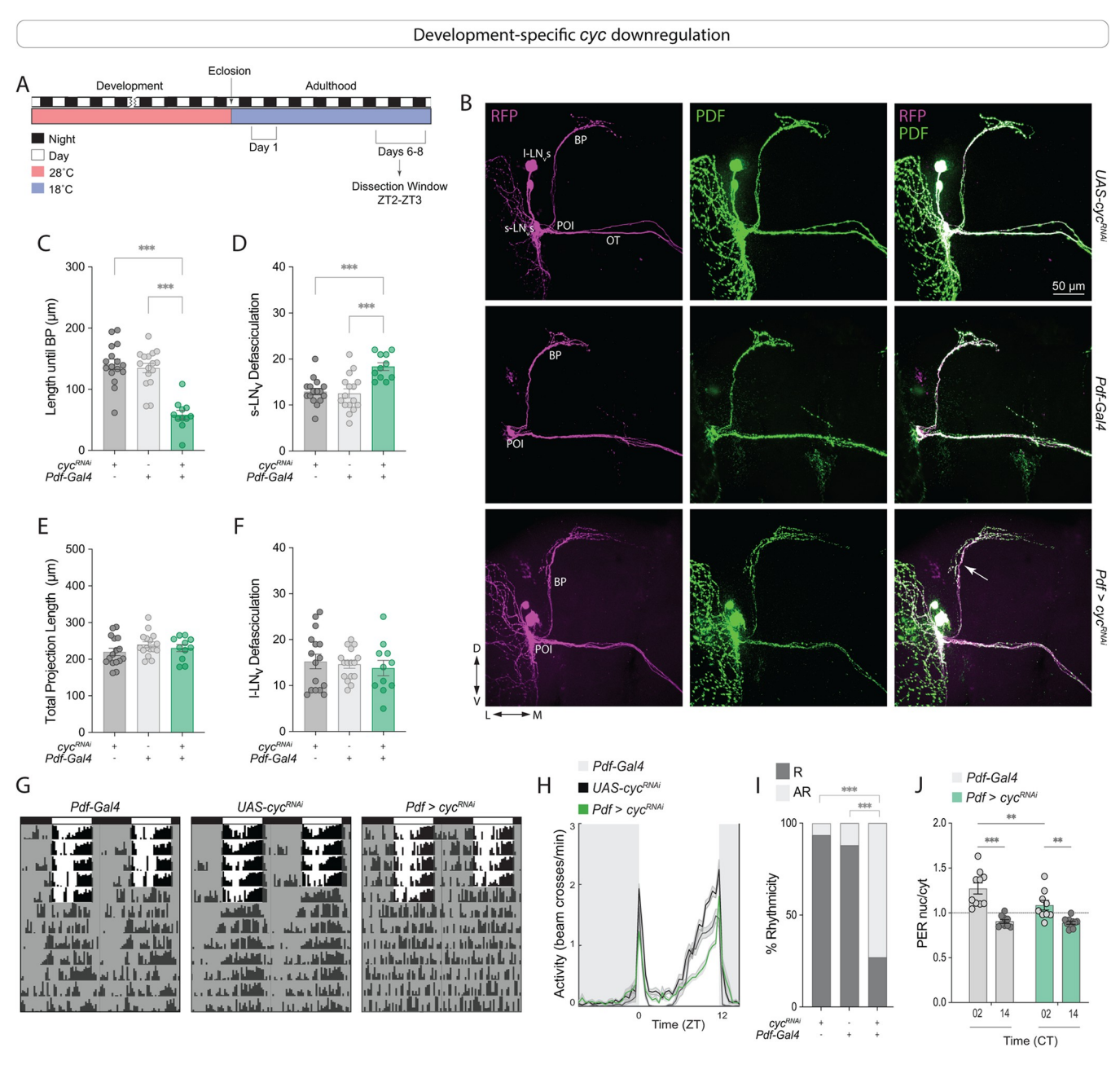


Fig 3. Development-specific cyc downregulation in Pdf+ cells prevents sLN_v fasciculation. (A) Representative timeline of the experiments in the figure. Flies were raised in LD at 28°C, and transferred to 18°C immediately after eclosion. Dissections were then performed in 6-8 day old adults at ZT2-3. (B) Representative confocal images of anti-PDF (green) and anti-RFP (magenta) staining of adult fly brains in which cyc was downregulated only during development. Each line also included a Pdf-RFP transgene. The white arrow indicates the increased defasciculation in the sLNv projections in experimental flies. Scale bar = $50 \mu m$. (C-F) Quantification of the LN_v morphology phenotypes of flies of the indicated genotypes. The driver line also included a tub- $Gal80^{ts}$ transgene. The sLN_v projection length until the branching point (BP) (C), the number of intersections of sLN_v ventral projections (D), the total sLN_v projection length (E), and the total number of intersections of the ILN_v projections along the optic tract (OT) (F) are shown for flies in which cyc was downregulated in Pdf + cells until eclosion. Two independent experiments were conducted. For each genotype: $11 \le n \le 16$. One-way ANOVA tests were used to quantify the LN_v morphology. *** p < 0.001. Error bars indicate SEM. Each dot corresponds to one brain. (G-I). Behavioral phenotypes of development-specific cyc knockdown. Flies were raised in LD at 28°C, before being transferred to 18°C upon eclosion. Experiments were conducted at 18°C. (G) Representative actograms of flies of the indicated genotypes under free-running (see Table 1 for n and additional quantifications). (H) Population activity plots for flies during days 3-5 of the LD cycle at 18°C. (I) Percent rhythmicity for the indicated genotypes under DD. R = Rhythmic and AR = arrhythmic. Fisher's exact contingency tests were used to analyze the percentage of rhythmic flies under DD (DD1-7). *** p < 0.001. Error bars indicate SEM. The data correspond to three independent behavior experiments. For each genotype: $68 \le n \le 94$. (J) Quantification of nuclear over cytoplasmic PER immunosignal within the sLN_vs on day 2 of constant darkness at 18°C from brains of Gal4 controls or cyc RNAi-expressing flies. A two-way ANOVA was employed for statistical analysis. ** p < 0.01, **** p < 0.001. Error bars indicate SEM.

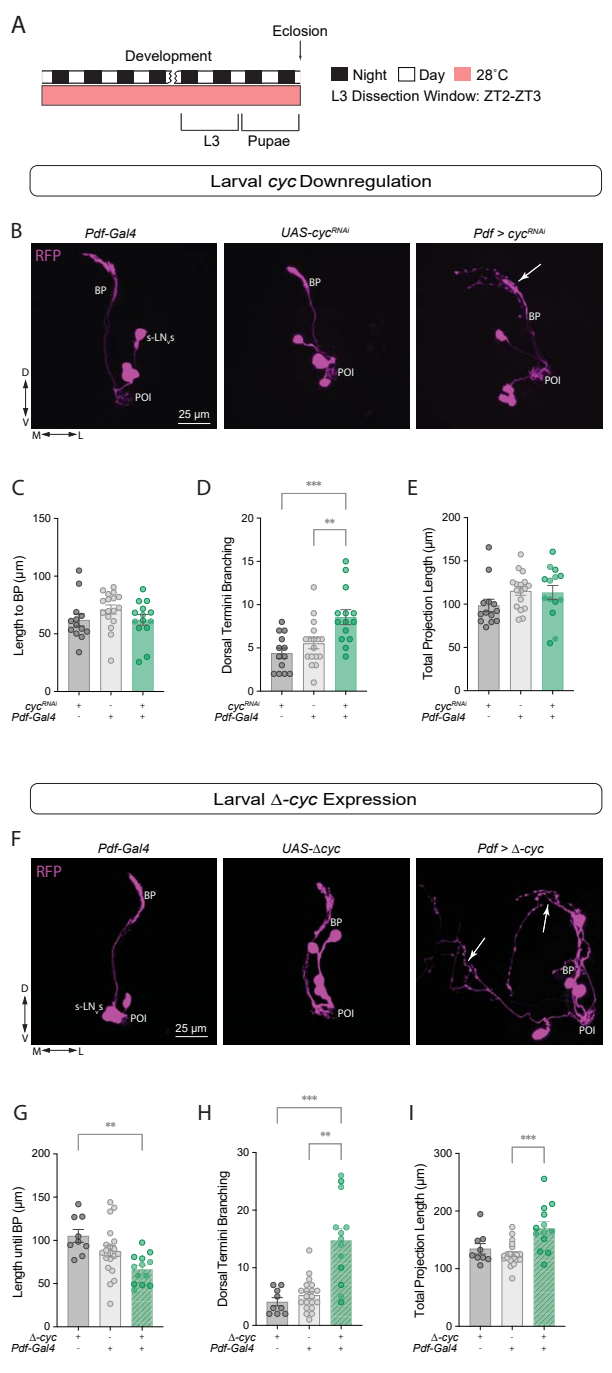


Fig 4. *Cyc* manipulations lead to aberrant sLN_v projections in larval clock neurons. (A) Representative timeline of the experiments in the figure. Larvae were raised in LD at 28°C. Third instar larvae (L3) were dissected at ZT2-3. (B-E) Developmental effects of *cyc* knockdown in the sLN_vs. (B) Representative confocal images of L3 larval brains stained with anti-RFP, labeling the sLN_vs. (C-E) The projection length from the POI to the BP (C), the degree of sLN_v dorsal termini branching (D), and the total projection length (E) were compared. For each genotype: $13 \le n \le 17$. (F-I) Developmental effects of expressing a dominant-negative form of *cyc*, Δ -*cyc*, in the larval sLN_vs. (F) Representative confocal images of anti-RFP staining in the sLN_vs of L3 larvae. A one-way ANOVA followed by a Tukey's Multiple Comparisons tests was used to compare the projection length from the POI to the BP (G). A Kruskal-Wallis tests followed by Dunn's multiple comparisons tests compared the nonparametric data sets: the degree of sLN_v dorsal termini branching (H) and the total projection length (I). Each dot corresponds to one brain. For each genotype: $9 \le n \le 20$.** p < 0.01, *** p < 0.001. Three independent experiments were conducted for each genetic manipulation and each line also included a *Pdf-RFP* transgene. The driver lines also included a *tub-Gal80*^{ts} transgene. Error bars indicate SEM.

branching point (S1B Fig; see methods section). The total sLN_v projection length was not affected by the genetic manipulation (Fig 4E).

Since the effects of cyc knockdown via RNAi and the expression of a cyc dominant negative form in adults were similar (Figs 1 and S2), we analyzed the morphology of the sLN_v projections in L3 larvae upon Δ -cyc expression. In $Pdf > \Delta$ -cyc larval brains, the length to the branching point was significantly lower (Fig 4F and 4G) and the number of branches was significantly greater than that of controls (Fig 4H). The total projection length was not affected (Fig 4I). Taken together, these results suggest that cyc plays a role in the development of the larval sLN_v neurons.

Clk downregulation increases sLNv dorsal arborizations

Clk and cyc mutations produce similar effects on the expression pattern of PDF in adult brains [23]. CLK and CYC act as heterodimeric transcriptional activators, and the circadian phenotypes associated with mutations in these core circadian clock genes, both molecular and behavioral, are largely similar [43, 47, 51]. To determine if downregulating Clk in the sLN_vs leads to the same defasciculation of the sLN_vs observed with cyc manipulations, we performed similar experiments as those described above, in which we expressed Clk^{RNAi} in Pdf+ neurons. We found that $Pdf > Clk^{RNAi}$ flies also showed neuronal morphology phenotypes (Fig 5).

In a previous study, Clk downregulation resulted in overfasciculation of the sLN_v dorsal termini when stained with anti-PDF [52]. However, RFP labeling of the sLN_v membrane indicated that these termini were actually more expanded than those of control flies, resulting in significantly higher dorsal termini branching (Figs 5B-5E and SLC). In $Pdf > Clk^{RNAi}$ flies, neither the distance to the branching point (Fig 5C) nor the degree of defasciculation differed from controls (Fig 5D). Neither the sLN_v total projection length nor the lLN_v projections were affected (S4C and S4D Fig). Only ~48% of the $Pdf > Clk^{RNAi}$ flies were rhythmic, and those that were rhythmic exhibited a lengthening of the free-running period (S4B Fig and Table 1). Nuclear PER levels in $Pdf > Clk^{RNAi}$ flies were significantly reduced in the LN_v s (S4H–S4J Fig).

Expression of Δ -Clk in the Pdf+ cells did not result in changes in the sLN_v projection length until branching point (Fig 5F and 5G) or the total length of the projections (S4F Fig). However, the $Pdf > \Delta$ -Clk brains had increased defasciculation of the ventral projection (Fig 5H). The degree of dorsal termini branching in the $Pdf > \Delta$ -Clk flies was not significant (Fig 5I), not was the degreed of lLN_v defasciculation (S4G Fig). Under DD at 28°C, the majority of Δ -Clk expressing flies were arrhythmic (S4E Fig), consistent with what was reported at 25°C [43].

We then examined L3 larval brains to determine if the observed phenotypes were already present at this developmental stage. While expression of Clk^{RNAi} did not result in morphological phenotypes in larval LN_vs (S5 Fig), expression of Δ -Clk resulted in pronounced phenotypes (Fig 6A and 6B). We observed a significant increase in sLN_v dorsal termini branching (Fig 6D) and total projection length (Fig 6E) in $Pdf > \Delta$ -Clk larvae. The length to the branching point for the experimental larvae was not significantly different from that of the control lines (Fig 6C). Expressing Δ -Clk led to more pronounced phenotypes in the larval stage than Clk down-regulation, possibly due to incomplete knockdown.

In addition to the main feedback loop, CLK and CYC form a secondary loop by activating vri and $Pdp1\varepsilon$ [8, 9], which repress and activate Clk expression, respectively. The low PDF peptide in the sLN_vs projections of cyc^{01} mutants can be rescued by vri overexpression [39]. To determine if vri expression also affects sLN_vs morphology we expressed a line with a CRISPR/ Cas9-based gRNA targeting the vri gene [53] under the control of the Pdf-Gal4 driver. We found that in Pdf > Cas9 + vri-g flies neither the distance until branching point in the s-L N_vs (Fig 7B and 7C) nor the degree of fasciculation of the s-L N_vs (Fig 7D) was different from

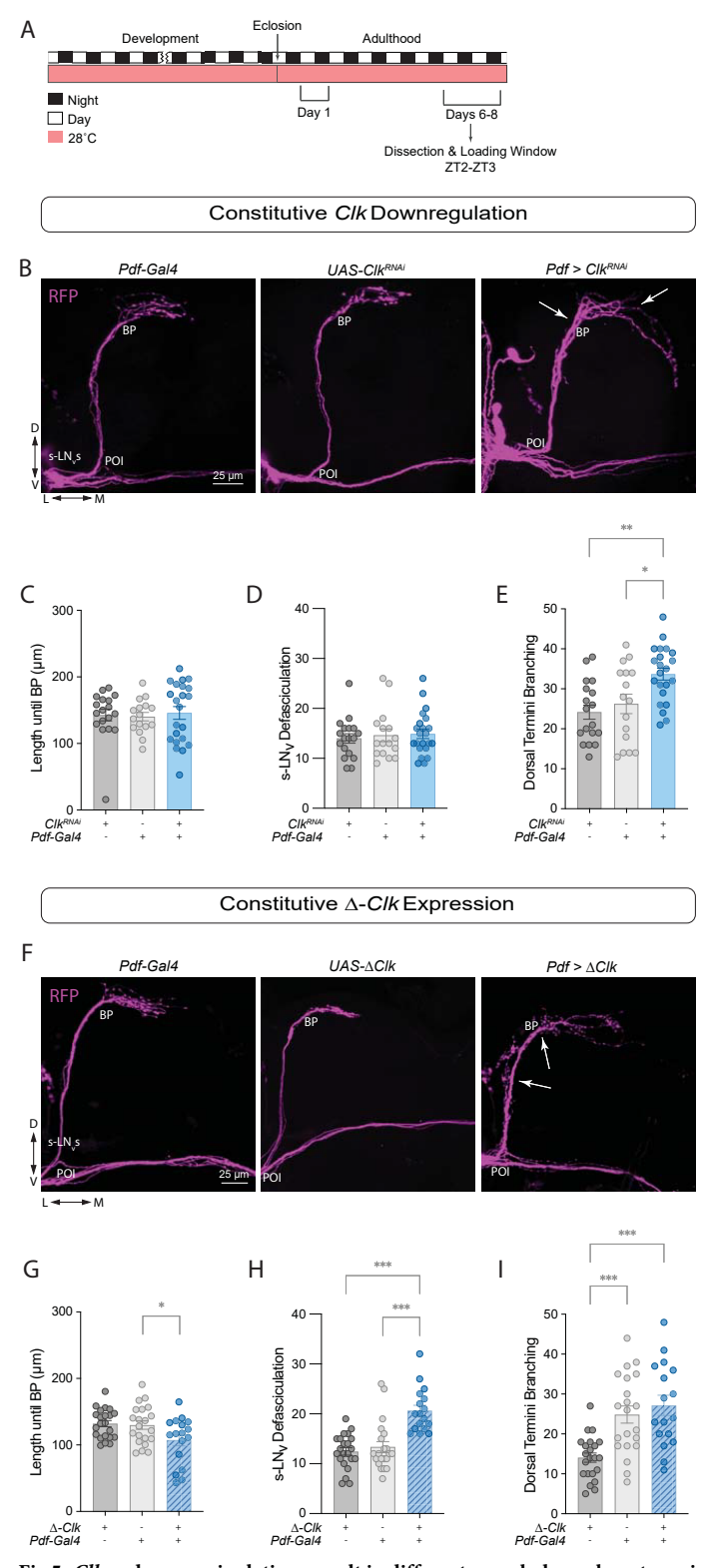


Fig 5. $\it Clk$ and $\it cyc$ manipulations result in different morphology phenotypes in clock neurons. (A) Representative timeline of the experiments in the figure. Flies were kept in LD conditions at 28°C for their entire lifespan. Dissections were performed within Days 6–8 post-eclosion at ZT2-3. (B) Representative confocal images of anti-RFP staining in the sLN_vs adult brains of control ($\it Clk^{RNAi}$ /+ and $\it Pdf$ - $\it Gal4$; $\it tub$ - $\it Gal80^{ls}$ /+), and experimental ($\it Pdf$) $\it Clk^{RNAi}$) flies. White arrows indicate the BP (left) and extension of some of the sLN_v dorsal projections (right) in the experimental

line. All lines employed also included a Pdf-RFP transgene. Scale bar = $25 \, \mu m$. (C-E) Quantification of sLN_v morphology using Kruskal-Wallis tests followed by Dunn's multiple comparisons tests for nonparametric datasets, compared the length until the branching point (C) and the total number of axonal crosses of the sLN_vs (D). For parametric data, ordinary one-way ANOVA tests followed by Tukey's Multiple Comparisons tests compared the total number of axonal crosses after the BP (E). Each dot corresponds to one brain. Two independent experiments were conducted. For each genotype: $16 \le n \le 22. * p < 0.05, *** p < 0.001$. Error bars indicate SEM. (F) Representative confocal images of anti-RFP (magenta) staining in the sLN_v s adult brains of control (UAS- ΔClk /+ and Pdf-Gal4;tub- $Gal80^{ts}$ /+), and experimental (Pdf > Δ -Clk) flies. White arrows indicate the BP (top) and increased defasciculation along the sLN_v projections (bottom). All lines employed also included a Pdf-RFP transgene. Scale bar = $25 \, \mu m$. (G-I) Quantification of sLN_v morphology phenotypes: length until the branching point (G), the total number of axonal crosses of the sLN_v s (H), and the total number of axonal crosses after the BP (I). For parametric data, ordinary one-way ANOVA tests followed by Tukey's Multiple Comparisons tests were employed. For nonparametric data, Kruskal-Wallis tests followed by Dunn's multiple comparisons tests were employed. See <u>S1 Table</u> for details about statistical analysis. Each dot corresponds to one brain. Two independent experiments were conducted. For each genotype: $17 \le n \le 22. * * p < 0.01, *** * p < 0.001$. Error bars indicate SEM.

https://doi.org/10.1371/journal.pgen.1011441.g005

controls. The total projection length was significantly higher than controls (Fig 7E), but in this case due to projections extending ventrally towards the optic tract (Fig 7B). In the majority of the brains, some s-LN $_{\rm v}$ projections extended towards the ventral brain after reaching the SMP (Fig 7B) and in most cases contacted the l-LNv contralateral projections in the optic tract (Fig 7F and 7G), a phenotype that was never observed in control brains.

Discussion

Our results reveal a role for the circadian clock gene cyc in establishing the proper cellular morphology of the key clock pacemaker neurons, the sLN_vs . Both constitutive cyc knockdown or expression of a dominant negative form of cyc in Pdf+ cells result in increased defasciculation of the sLN_vs . In addition, Clk downregulation and expression of a dominant negative form of Clk also result in sLN_v morphology phenotypes, although some of those phenotypes appear to be distinct from those caused by cyc manipulations. Expressing the dominant-negative forms of either Clk or cyc has been used in previous studies as an effective way to prevent molecular oscillations in subsets of clock neurons. However, our results indicate that these genetic manipulations lead to additional morphological phenotypes beyond molecular time-keeping that are already detectable during the larval stages.

In addition to anatomical and functional classifications, clock neurons can be divided into early or late developmental groups depending on when circadian oscillations can be detected. In the early groups, which include the sLN_vs, *per* and *tim* expression rhythms can be detected at the first instar (L1) larval stage, whereas in the late groups, such rhythms cannot be detected until metamorphosis [25, 54]. However, *cyc* and *Clk* expression using GFP-*cyc* and GFP-*Clk* transgenes can be detected in almost all groups of clock neurons at early developmental stages, even days before *per* oscillations begin [10]. This suggests that *cyc* and *Clk* play additional roles in the development of clock neurons beyond their role in the molecular oscillator.

Both cyc and Clk modulate PDF expression in both larval and adult clock neurons. In $Clk^{\rm jrk}$ mutants, neither PDF nor Pdf mRNA can be detected in most larval [32] or adult sLN_vs [23], and similar effects have been observed for the cyc^{02} mutant [23]. However, around half of the cyc^{01} brains stained with PDF exhibit 'stunted' sLNv projections which appear to lack their dorsal termini [40]. This study by Goda et al. also showed that panneuronal rescue of cyc expression throughout development is sufficient to restore PDF expression in the LN_v dorsal projections of cyc^{01} mutants [40]. Overexpression of vri, a clock gene that is downstream of CLK/CYC and acts as a repressor of CLK transcription [9, 32], causes a severe reduction in PDF levels in larval brains [32], and the low PDF levels in the sLN_vs of cyc^{01} mutants can be

Table 1. Summary of free running activity rhythms. Related to Figs 2, 3, and 7 and \$1-\$4. Activity analysis of the above genotypes at 25°C, 28°C, or 18°C. Light conditions for each experiment was 12:12 LD for 5 days followed by DD for at least 8 days. Depending on the experiment, flies were raised at 25°C, 28°C, or 18°C. Flies raised a 25°C were kept at that temperature throughout the behavior experiment. Flies raised at 18°C were transferred to 28°C upon eclosion and behavior experiments were conducted at 28°C. Flies raised at 28°C were either kept at 28°C for behavior experiments (constitutive knockdown) or transferred to 18°C upon eclosion (development-specific knockdown). ClockLab's \(\chi_{\text{square}} \) eriodogram analysis was used to analyze rhythmicity, rhythmic power, and free-running period for each above genotypes. The \(\text{%} \) rhythmicity along with the number of rhythmic flies (nR), the period in hours with the SEM, and the rhythmic power with the SEM are indicated. Arrhythmic flies were not included in the analysis of period or power.

Temperature pre-eclosion: 28°C, Temperature post-eclosion: 28°C					
Genotype	Number of Flies (n)	% Rhythmicity (nR)	Period (h) ± SEM	Rhythmic Power ± SEM	
;Pdf-Red,Pdf-Gal4;Tub-Gal80 ^{ts}	40	97.50 (39)	24.44 ± 0.06	109.80 ± 6.39	
;UAS-cyc ^{RNAi} ⁴²⁵⁶³ ;	48	85.42 (41)	24.02 ± 0.08	85.74 ± 7.91	
;Pdf-Red,Pdf-Gal4;Tub-Gal80 ^{ts} >; UAS-cyc ^{RNAi} 42563;	40	10.00 (4)	25.88 ± 3.03	24.32 ± 3.71	
;UAS-Clk ^{RNAi 42566} ;	26	92.31 (24)	23.73 ± 0.10	97.66 ± 8.90	
;Pdf-Red,Pdf-Gal4;Tub-Gal80 ^{ts} >; UAS-Clk ^{RNAi} 42566;	21	52.38 (11)	25.36 ± 0.22	36.74 ± 6.76	
;Pdf-Red,Pdf-Gal4;Tub-Gal80 ^{ts}	24	100.00 (24)	24.5 ± 0.07	101.40 ± 8.97	
;UAS-cas9/CyO; UAS-Vrig/TM6b Tb	16	87.50 (14)	23.86 ± 0.11	124.6 ± 10.39	
;Pdf-Red,Pdf-Gal4;Tub-Gal80 ^{ts} >; UAS-cas9/CyO; UAS-Vrig/TM6b Tb	18	38.89 (7)	23.50 ± 0.15	29.02 ± 3.68	
;Pdf-Red,Pdf-Gal4;Tub-Gal80 ^{ts}	31	83.87 (26)	24.98 ± 0.07	56.76 ± 6.73	
;UAS-Δcyc;	24	95.83 (23)	23.54 ± 0.08	72.79 ± 9.29	
;Pdf-Red,Pdf-Gal4;Tub-Gal80 ^{ts} >; UAS-∆cyc;	32	3.13 (1)	25.50 ± 0.00	13.66 ± 0.00	
;UAS-∆Clk	27	100.00 (27)	23.52 ± 0.06	93.52 ± 8.71	
;Pdf-Red,Pdf-Gal4;Tub-Gal80 ^{ts} >; UAS-∆Clk	28	3.57 (1)	23.50 ± 0.00	17.18 ± 0.00	

Temperature pre-eclosion: 28°C, Temperature post-eclosion: 18°C

Genotype	Number of Flies (n)	% Rhythmicity (nR)	Period (h) ± SEM	Rhythmic Power ± SEM
;Pdf-Red,Pdf-Gal4;Tub-Gal80 ^{ts}	68	88.24 (60)	24.40 ± 0.17	87.80 ± 7.33
;UAS-cyc ^{RNAi} 42563;	94	93.62 (88)	24.18 ± 0.04	81.06 ± 4.38
;Pdf-Red,Pdf-Gal4;Tub-Gal80 ^{ts} >; UAS-cyc ^{RNAi} 42563;	70	27.14 (19)	23.82 ± 0.81	21.42 ± 1.78
Tempera	ature pre-eclosion: 1	8°C, Temperature post-ecl	osion: 28°C	·
Genotype	Number of Flies (n)	% Rhythmicity (nR)	Period (h) ± SEM	Rhythmic Power ± SEM
;Pdf-Red,Pdf-Gal4;Tub-Gal80 ^{ts}	30	100 (30)	24.93 ± 0.04	127.8 ± 6.76
;UAS-cyc ^{RNAi} 42563;	25	96 (24)	24.04 ± 0.07	150.1 ± 12.44
;Pdf-Red,Pdf-Gal4;Tub-Gal80 ^{ts} >; UAS-cyc ^{RNAi} 42563;	31	38.71 (12)	23.67 ± 0.61	24.27 ± 3.68
Tempera	ature pre-eclosion: 2	5°C, Temperature post-ecl	osion: 25°C	·
Genotype	Number of Flies (n)	% Rhythmicity (nR)	Period (h) ± SEM	Rhythmic Power ± SEM
;Pdf-Red,Pdf-Gal4;	29	89.66 (26)	24.52 ± 0.08	152.2 ± 11.53

83.87 (26)

12.90 (4)

31

31

https://doi.org/10.1371/journal.pgen.1011441.t001

;Pdf-Red,Pdf-Gal4; >; UAS-cyc^{RNAi} 42563;

;UAS-cycRNAi 42563;

rescued by vri overexpression [39]. However, restoring PDF expression in the sLN_vs in flies lacking vri expression is not sufficient to rescue activity rhythms.

 24.06 ± 0.08

 23.13 ± 0.24

Unlike in cyc and Clk mutants [23], PDF can be detected in the sLN_vs projections in per⁰¹ and tim⁰¹ mutants, although it no longer shows rhythms in its accumulation in the dorsal termini [23]. In addition, structural plasticity rhythms in the sLN_vs are absent in both per⁰¹ and tim^{01} mutants [27]. Downregulation of Clk [52], expression of Δ -cyc [30], and overexpression of vri in Pdf-expressing cells [39] also result in impaired plasticity rhythms [55]. Although the

 95.44 ± 9.61

 21.55 ± 6.93

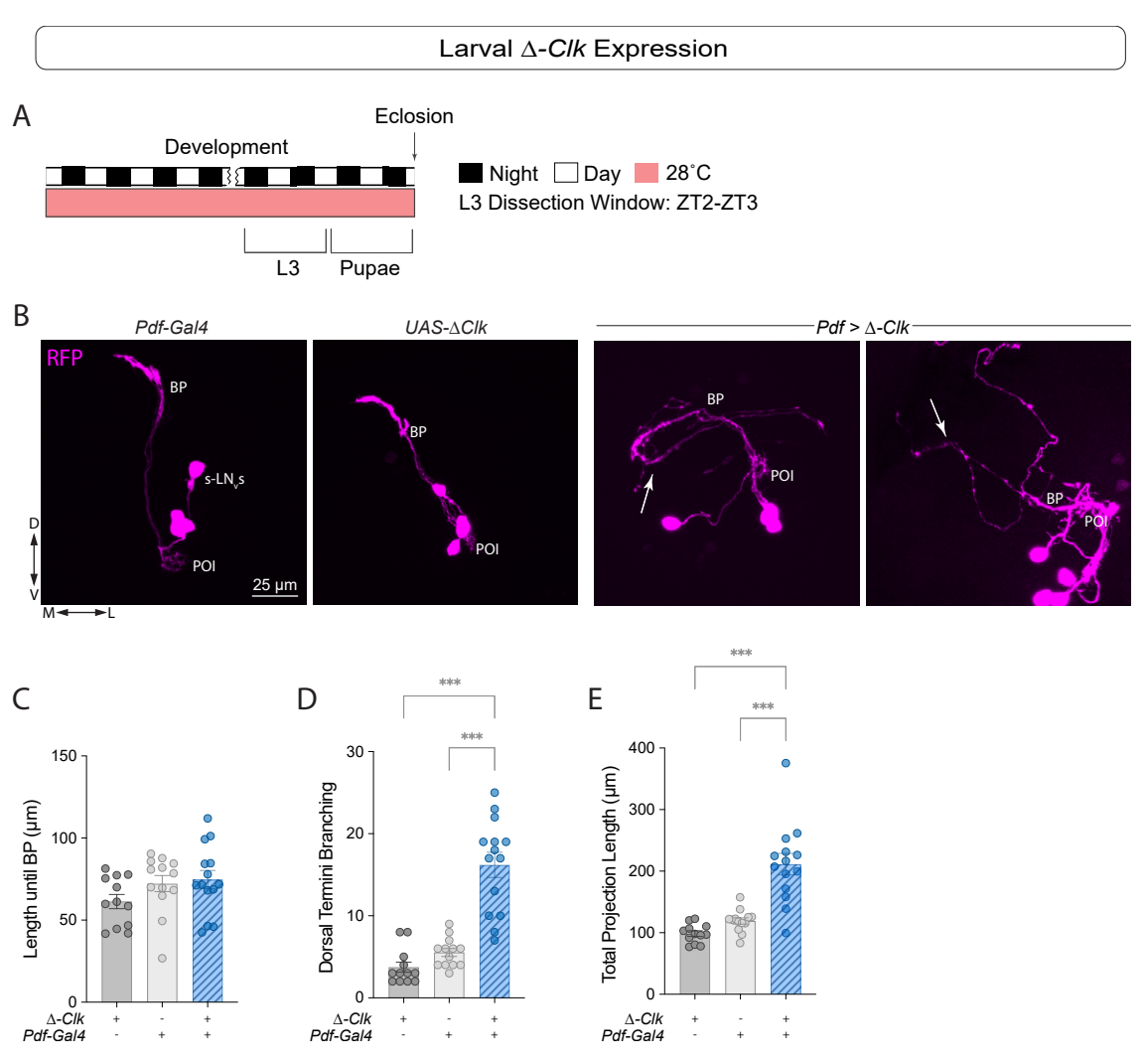


Fig 6. Expressing Δ-Clk in the sLN_vs leads to axonal morphology phenotypes in L3 larvae. (A) Representative timeline of the experiments in the figure. Larvae were raised in LD at 28 °C. Third instar larvae (L3) were dissected at ZT2-3. (B) Representative confocal images of anti-RFP (magenta) staining in the sLN_vs when Δ -Clk was expressed in Pdf+ neurons in L3 larvae. Each line also included a Pdf-RFP transgene, and the driver line also included a tub-Gal80^{ts} transgene. White arrows indicate misrouting of the sLN_v projections in the experimental line. Scale bar = 25 μm. For nonparametric data, Kruskal-Wallis tests followed by Dunn's multiple comparisons tests were used to compare the length to the BP (C). One way ANOVA tests were used to compare dorsal termini branching (D) and the total projection length (E). Two independent experiments were conducted. Each dot corresponds to one brain. For each genotype: $12 \le n \le 14$. **** p < 0.001. Error bars indicate SEM.

anatomical phenotypes seen in these mutants are milder than those that observed when cyc and Clk are downregulated or when their dominant negative forms are expressed, the $\rm sLN_v$ projections of both per and tim null mutants also exhibit altered morphology [27].

Our results suggest that Clk and cyc manipulations produce different phenotypes, however, it is possible that this is partially due to a less effective knockdown of Clk. Behavioral experiments show that cyc knockdown in Pdf+ neurons result in a larger fraction of arrhythmic flies than knockdown of Clk (Table 1). Use of RNAi often reduces gene expression but does not completely eliminate it, and may lead to off-target side effects. In addition, RNAi efficiency may vary over time. Expression of dominant negative alleles was used as an independent approach, but this method has limitations as well: over-expression levels for cyc and Clk may

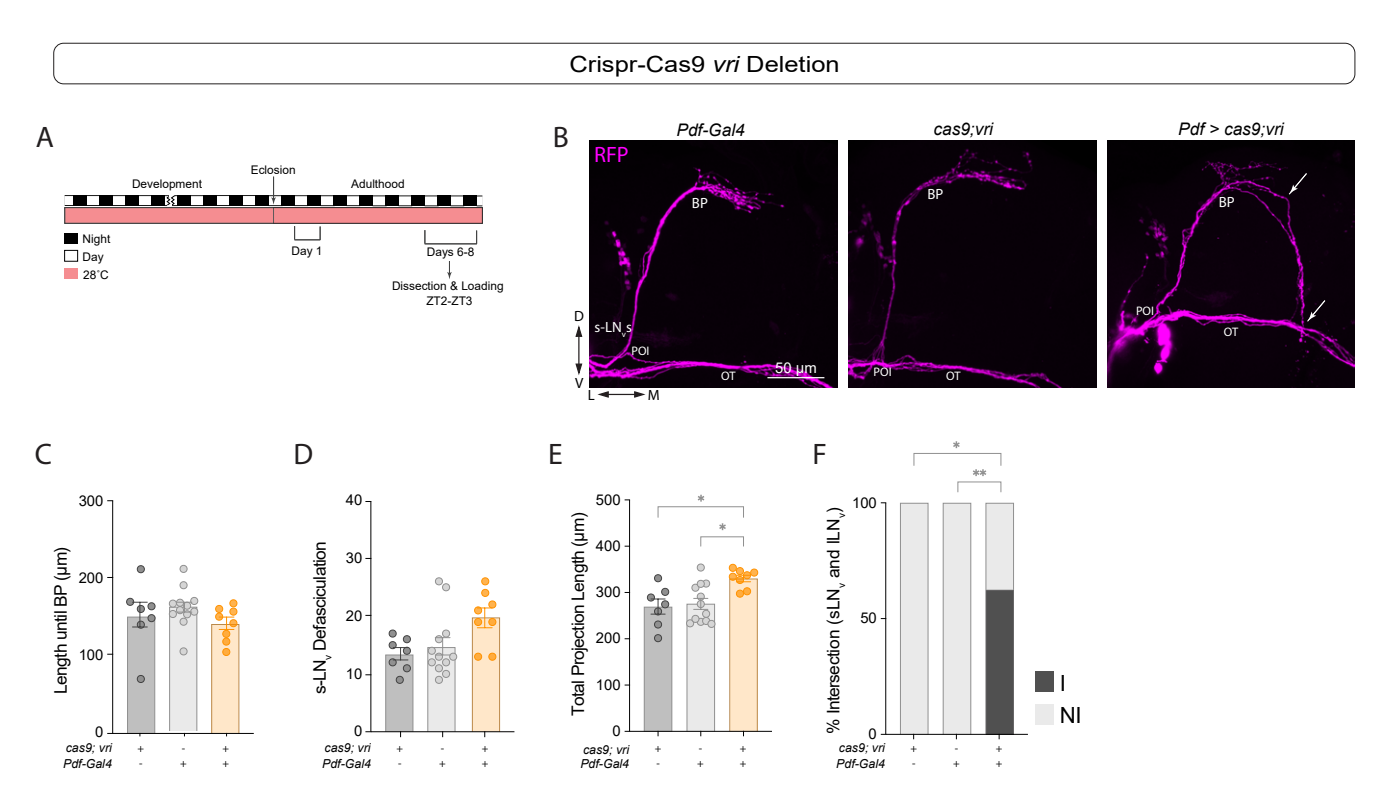


Fig 7. Vri mutagenesis results in sLN_v hyperextension. (A) Representative timeline of the experiments in the figure. Flies were kept in LD conditions at 28° C for their entire lifespan. Dissections were performed in 6-8 day old adults at ZT2-3. Behavioral experiments were run at constant 28° C. (B) Representative confocal images of anti-RFP (magenta) staining in the sLN_v s adult brains of control (cas9;vrig)+ and Pdf-Gal4;tub- $Gal80^{fs}$ +), and experimental (Pdf > cas9;vrig) flies. All lines employed also included a Pdf-RFP transgene. White arrows indicate the misrouting of the sLN_v dorsal projections (top), and the intersection of the sLN_v with the ILN_v s at the OT (bottom). Scale bar = $25 \mu m$. (C-E) Kruskal-Wallis tests followed by Dunn's multiple comparisons tests were used to compare the length until the branching point (C), the total number of intersections of the sLN_v s ventral projections (D), and the longest path of the sLN_v projections (without including misrouting) (E). (F) Fisher's exact contingency tests were used to analyze the percentage of brains where the sLN_v s intersected with the ILN_v s at the optic tract (I = Intersecting, N.I. = Not Intersecting). See Table 1 for additional quantifications. Each dot corresponds to one brain. Two independent experiments were conducted. For each genotype: $7 \le n \le 12$. * p < 0.05, ** p < 0.01, *** p < 0.001. Error bars indicate SEM.

differ, and non-native molecular interactions may occur at high concentrations. However, differential effects of cyc and Clk mutations have been previously described: cyc^{01} and Clk^{jrk} mutants showed differences in their sleep consolidation during the day and in their ability to recover after sleep deprivation [47].

CYC/CLK may regulate neuronal fasciculation by modulating the expression of genes involved in cell migration or cytoskeletal dynamics. For example, increasing matrix metalloproteinases 1 (MMP1) expression reduces the complexity of the sLNv arborizations along the projections [31]. MMP1 promotes fasciculation in *Drosophila* motor neuron axons [56]. *Clk* has been shown to affect sLNv dorsal termini arborization through the activation of Mef2, which negative regulates Fas2 expression [52]. Our results from *Clk* downregulation show increased rather than decreased sLNv dorsal termini arborization. One important difference is that we used RFP to label the membrane rather than a PDF staining. As for *cyc*, among the sLNv morphology phenotypes reported in the literature, including those of other clock mutants, PDF/PDFR [57], and Rho GTPases [28], among others, the phenotype most similar to *cyc* downregulation is the downregulation of the *Medea (Med)*. Med is homolog of the human tumor-suppressor gene *DPC4* and is involved in the *decapentaplegic (dpp)* pathway [58], and its downregulation via RNAi in *Pdf*+ neurons results in decreased fasciculation along

the projections of the sLNvs [57]. In addition, similar to *cyc* manipulations, developmental specific downregulation of Med leads to morphology phenotypes in adult clock neurons [57].

Expression of *Clk* outside the clock network leads to the generation of ectopic clocks [59], but they require cyc expression. A study by Liu et al. showed that Clk stabilizes CYC both in cultured Drosophila Schneider 2 (S2) cells and in vivo: upon ectopic Clk expression, GFP-CYC can be detected in additional cells beyond the clock neuron network, suggesting that although with this reporter the CYC protein could be detected in the brain only in clock neurons, cyc mRNA is more broadly expressed [60]. In addition, cyc mRNA was not enriched in the LNvs compared to other elav-expressing neurons in the head [61]. Single cell RNA sequencing data revealed that cyc mRNA is present in non-clock neurons as well as in various tissues throughout the fly's body, with particularly high expression in the gut, ovaries, and testes [62]. In some instances, cyc mRNA expression levels are very high while Clk mRNA levels are low, such as in intestinal stem cells and the chordotonal organ [62]. The role of cyc mRNA expression in nonclock cells remains unknown. An interesting question for future studies is whether CLK and CYC act as an obligate heterodimer in their neurodevelopmental function and other possible non-circadian roles. In mammals, BMAL1 can dimerize with NPAS2 in addition to CLOCK [63], and a recent study in *Drosophila* detected co-binding of CYC and FOXO in the promoter region of vrille [64]. Single seq RNA sequencing in the sLNvs and other clock neurons, comparing the effects of cyc vs Clk downregulation, could help clarify the degree to which they function independently. Our results suggest that Clk and cyc are involved in shaping the morphology of clock neurons, and it is possible that they play similar roles in non-clock neurons as well.

Materials and Methods

Fly lines and rearing

Flies were raised on cornmeal-sucrose yeast media in a Percival Incubator under 12:12 LD at different temperature conditions. Depending on the experiment, flies were raised under either 18°C, 25°C, or 28°C (indicated in the figure legends). The lines *UAS-cyc*^{RNAi} (BDSC #42563), *UAS-Clk*^{RNAi} (BDSC #42566), *w*¹¹¹⁸ (BDSC #3605) and CS (BDSC #64349) were obtained from the Bloomington *Drosophila* Stock Center. The lines *Pdf-RFP,Pdf-Gal4;Tub-gal80*^{ts} and *w;Pdf-RFP;MKRS/TM6* were donated by Justin Blau (New York University). The *cyc*⁰¹, UAS-Δ-cyc, and UAS-Δ-Clk stocks were donated by Paul Hardin (University of Texas).

Immunohistochemistry

LN_v PDF levels and neuronal morphology. Brains of 6–8-day-old adult males or L3 larvae were dissected between ZT2 and ZT3 in ice-cold Schneider's *Drosophila* Medium (S2) (Thermo Fisher, #21720024). They were fixed immediately after dissection in 2% Paraformal-dehyde (PFA) in S2 for 30 minutes. Brains were then treated with blocking solution (5% goat serum in 0.3% PBS-Tx) for 1 hour at room temperature followed by incubation with primary antibodies at 4°C for 24–48 hr. The primary antibodies used were 1:3000 mouse anti-PDF (Developmental Hybridoma Bank) and 1:1000 rabbit anti-RFP (Rockland, #600-401-379-RTU). After incubation, the brains were rinsed 6 times in 0.3% PBS + Triton X-100 (PBT), after which they were incubated with Alexa-fluor conjugated secondary antibodies for 24-hr at 4°C. The secondary antibodies used were 1:3000 Alexa-488 (Thermo Fisher, #A11029) and 1:1000 Alexa-568 (Thermo Fisher, #A11036). The brain samples were further washed 6 times with 0.3% PBT, cleaned and mounted on a clean glass slide in Vectashield (Vector Laboratories, #H-1000-10) mounting media. A list of reagents can be found on Table 2.

Table 2. List of reagents.

REAGENT or RESOURCE	SOURCE	IDENTIFIER
Experimental Models: Organisms/Strains		
w;Pdf-RFP,Pdf-Gal4;Tub-gal80 ^{ts}	J. Blau, NYU	
w;Pdf-RFP;MKRS/TM6	J. Blau, NYU	
;UAS-∆Clk #1	J. Blau, NYU	
W;UAS-cas9/CyO;UAS-Vrig;TM6b Tb	M.Rosbash, Brandeis	
w;;UAS-cyc ^{RNAi42563}	Bloomington Drosophila Stock Center	BDSC 42563
w;;UAS-Clk ^{RNAi 42566}	Bloomington Drosophila Stock Center	BDSC 42566
w ¹¹¹⁸ ;+;+	Bloomington Drosophila Stock Center	BDSC 3605
Canton-S	Bloomington Drosophila Stock Center	BDSC 64349
сус ⁰¹	P. Hardin, University of Texas	BDSC 80929
;UAS-Δcyc;	P. Hardin, University of Texas	
;UAS-∆Clk	P. Hardin, University of Texas; Bloomington Drosophila Stock Center	BDSC 3618
Antibodies		
Rabbi anti-RFP (1:1000)	Rockland	#600-401-379-RTU
Mouse anti-PDF (1:3000)	Developmental Hybridoma Bank	
Rat anti-PER (1:500)	O. Shafer (ASRC CUNY)	
Anti-rabbit Alexa-568 (1:1000)	Thermo Fisher	A11036
Donkey anti-rat Alexa-488 (1:500)	Thermo Fisher	A21208
Anti-mouse Alexa-488 (1:3000)	Thermo Fisher	A11029
Software		
Fiji	http://fiji.sc	RRID: SCR_002285
MATLAB R2022b	MathWorks, Natick	RRID: SCR_001622
GraphPad Prism 9.0	GraphPad Software	RRID: SCR_002798
DAM FileScan	Trikinetics	
ClockLab	Actimetrics	RRID:SCR_014309
Chemicals, Peptides, and Recombinant Protein	is	
Vectashield Mounting Medium	Vector Laboratories	#H-1000-10
Premix PBS Buffer (10x)	Sigma-Aldrich	Cat# 11666789001
2% Paraformaldehyde (PFA)	Sigma-Aldrich	47608-250ML-F
Triton- X-100	Bio Basic	CAS#9002-93-1
Schneider's <i>Drosophila</i> Medium (S2)	Thermo Fisher	21720024
Other		
DAM2 Drosophila Activity Monitors	Trikinetics	
DAM Drosophila Environmental Monitors	Trikinetics	

PER Staining. Brains of 6–8-day-old males were dissected one hour before lights-on (ZT23) in ice-cold Schneider's *Drosophila* Medium (S2) (Thermo Fisher, #21720024). Immediately after dissection, brains were fixed in 2% paraformaldehyde (PFA) for 30 minutes, stained and mounted as described above. The primary antibodies used were 1:1000 rabbit anti-RFP (Rockland, #600-401-379-RTU) and 1:500 rat anti-PER (donated by Orie Shafer). The secondary antibodies used were 1:1000 Alexa-568 (Thermo Fisher, #A11036) and 1:500 Alexa-488 (Thermo Fisher, #A21208).

For the analysis of PER subcellular localization (Fig 3J), flies were raised at 28C under LD and transferred to 18°C immediately after eclosion. After 5 days under LD 18C, flies were transferred to constant darkness at 18°C and brains were dissected on the second day of DD (DD2).

Imaging, quantification, and statistical analysis

All images were acquired on an Olympus Fluoview 1000 laser-scanning confocal microscope using a 40x/1.10 NA FUMFL N objective (Olympus, Center Valley, PA) at the Advanced Science Research Center (ASRC-CUNY). For all the experiments, only one hemisphere per brain was imaged (the right hemisphere, unless it was damaged, in which case we imaged the left hemisphere).

Quantification of adult LN_v morphology (sLN_v and lLN_v): We quantified 1) sLN_v total projection length, 2) sLN_v length from the point of origin (POI) until the branching point (BP) ('length until BP'), 3) the degree of defasciculation of the sLN_v ventral projections, 4) the sLN_v dorsal termini branching, 5) the degree of defasciculation of the l-LNv projections, and 6) intersections between sLN_v projections and lLN_v projections along the optic tract.

1-Total projection length: The total length of the dorsal projection was determined by a line drawn from the point of intersection (POI) between the sLN_vs and the optic tract until the end of the dorsal termini. If the projection length went past the midline of the brain, the length was measured up to the midline.

2-Length until BP: The partial length of the dorsal projections was determined by a line drawn from the POI until the BP of the $\rm sLN_v s$ at the dorsal termini. The projection length and partial projection length of the $\rm sLN_v s$ were quantified using Fiji in ImageJ.

3- Defasciculation of the sLN_v ventral projections (' sLN_v Defasciculation'): A modified Scholl's analysis [42], was used to analyze the degree of defasciculation of the ventral area of the sLN_v projections, near the cell bodies. Six concentric circles, each 25 μ m apart, were placed centered in the POI (S1C Fig). Each intersection between an individual ventral projection and any of the 6 circles was counted. A value of '10' denotes 10 total intersections between any of the projections and any of the circles.

4-sLNv Dorsal termini branching: A modified Scholl's analysis was used to analyze the degree of defasciculation of the dorsal termini of the sLN_v projections. This method is similar to what was previously described to quantify sLNv dorsal termini [27]. In this study, 8 concentric circles, each 12.5 um apart, were centered in the BP (S1E Fig). Each intersection between an individual dorsal projection and any of the 8 circles was counted. A value of '10' denotes 10 total intersections between any of the dorsal projections and any of the circles.

5-Defasciculation of the lLN_v optic tract projections. The degree of defasciculation of the lLNvs was determined using the same 6 concentric circles centered in the POI what were used to quantify defasciculation of the sLN_v ventral projections (2) (S1C Fig). Each intersection between an individual lLNv projection and any of the 6 circles was counted.

6- Intersections between sLN_v projections and lLNv projections along the optic tract. We quantified the percentage of brains in which at least one sLNv dorsal projection turned ventrally and extended towards the optic tract, contacting at least one lLNv projection. This phenotype was not observed in brains of control flies but was present in more than half of the brains of flies in which vri was knocked out (shown in Fig 7F).

Quantification of larval sLN_v morphology. We quantified the total projection length of the sLN_vs, the axonal projection length until the branching point of the and the degree of branching in the sLN_v dorsal projections (S1D Fig). The projection length, partial projection length, and area of the sLN_vs were quantified using Fiji. The projection length was measured by a line drawn from a determined first point of intersection (POI) of each of the sLN_v cell bodies until the end of the dorsal termini. The partial length of the axonal projections was determined by a line drawn for the same point of intersection until the branching point (BP) of the sLN_vs at the dorsal termini. A modified Scholl's analysis was used to measure the branching of the sLN_v projections. Six concentric circles were placed around the same

branching point used in the length measurements. The concentric circles were each 12.5 μ m away from each other, so that the farthest circle was 75 μ m away from the POI. The number of visible neurites of the sLN_vs that intersected with each circle were counted and summed, yielding the total number of intersecting neurons for the dorsal projections.

Quantification of PER levels. Single optical sections of either $sLN_v s$, $lLN_v s$ or $LN_d s$ were imaged using the same settings using a 40x/1.10 objective. PDF was used to identify the small and large $LN_v s$. The $LN_d s$ were identified based on their localization, size, and morphology. PER levels were determined through normalization of nuclear staining within each cell to the background. The average value for each brain within a cluster was computed by averaging the values obtained from multiple cells within that cluster. Quantification was performed using images from 5–6 brains per each cluster at each timepoint. For the analysis of PER subcellular localization (Fig 3]), the ratio of nuclear vs cytoplasmic PER levels was determined for individual sLNvs and compared using a two-way ANOVA.

Locomotor activity rhythm recording and analysis

DAM2 Drosophila Activity Monitors (TriKinetics, Waltham, MA) were used to record the locomotor activity rhythms of adult male flies aged three- to five-days, as previously described [65]. Flies were entrained to 12:12 LD cycles for at least five days, and then transferred to constant darkness (DD) for at least eight days at a constant temperature of 28°C, unless otherwise specified. Free-running activity rhythms were analyzed with ClockLab software from Actimetrics (Wilmette, IL). We employed ClockLab's χ-square periodogram function, which was integrated into ClockLab software, for the analysis of rhythmicity, rhythmic power, and freerunning period in individual flies, using a confidence level of 0.01 [33]. For each of the tested genotypes, only significant periodicities falling within the 14 to 34-hour range were taken into consideration. In instances where an individual fly exhibited multiple periodicities with peaks surpassing the significance threshold, only the period with the highest amplitude was utilized when calculating the average periods presented in Table 1. ClockLab assigns each peak in the χ-square periodogram both a "Power" value and a "Significance" value. The "Rhythmic Power" for each designated rhythmic fly was determined by subtracting the "Significance" value from the "Power" value associated with the predominant peak. Flies that did not exhibit a periodicity peak above the threshold (10) were categorized as "arrhythmic," and their period and rhythmic power were not included in the analysis [65].

Statistical analysis

Pearson's D'Agostino normality tests were performed for all the datasets. Depending on whether the data were normally distributed, statistical analyses were performed using either a one-way ANOVA with a Tukey's multiple comparisons test or a Kruskal-Wallis test with a Dunn's multiple comparisons test for 3 or more groups, or a t-test for comparisons between 2 groups. Fisher's exact contingency tests were run to analyze the percent rhythmicity for the indicated genotypes under DD.

Supporting information

S1 Fig. Quantification of LNvs defasciculation (ventral projections) and branching (dorsal projections). (A-B) The cyc^{01} mutant has disrupted sLN_v morphology. (A) Representative confocal images of anti-PDF staining in Canton-S control and cyc^{01} adult male brains. The sLN_v s and optic tract (OT) are indicated. Scale bar = 25 μ m. The inserts on the right show the sLN_v projections with the signal intensity adjusted for visibility in the cyc^{01} mutants. The top insert shows the distal (dorsal) area and the bottom insert shows the proximal (ventral) area of

the sLN_v projections. Scale bar = 10 µm. (B) Representative images of eight brains of; Pdf-RFP; cyc⁰¹ experimental flies stained with anti-RFP (magenta). Flies were raised at 28°C. Most of cyc⁰¹ mutant flies (~78.5%, 11 out of 14 brains) exhibit severe phenotypes in their sLNv morphology compared to the effects of cyc downregulation in Pdf+ neurons. (C-E) Representative confocal images of adult (C, E) and L3 larvae (D) control brains stained with anti-RFP (magenta). (C) To determine the degree of defasciculation of the sLN_v ventral projections in adult brains, 6 concentric circles separated by is 25 µm were centered at the point of intersection (POI), where the projections of the sLN_vs and those of the lLN_vs intersect. The most distant circle does not reach the main branching point (BP) in control brains; therefore, the dorsal termini are not included. The number of intersections between either the sLNvs or the lLN_vs and each concentric circle were quantified. (D) Dorsal projection branching in the larval sLN_vs was measured by counting the number of intersections the sLN_vs had at each of the 6 concentric circles separated by 12.5 µm. (E) Adult sLN_v dorsal projection branching was measured by counting the number of intersections the sLN_vs had at each of 8 concentric circles separated by 12.5 μm. This was adapted from a previous study [27] to capture the hyperextended projection phenotype of $Pdf > \Delta$ -Clk flies. (F-I) Quantification of the LN_v morphology phenotypes of experimental flies in which a cyc^{RNAi} transgene was driven by a; Pdf-RFP,Pdf-Gal4; driver compared to the parental controls. Flies were raised at 25°C. The sLN_v projection length until the branching point (BP) (F), the total number of intersections of the sLN_v ventral projections (G), the total sLN_v projection length (H), and the total number of intersections of the lLN_v projections along the optic tract (OT) (I) are shown. Graphs are representative of two independent experiments, with each dot representing one brain. For each genotype, n falls in the range: $18 \le n \le 21$. (I-J). **p < 0.01, *** p < 0.001. Error bars indicate SEM. See S1 Table for additional quantifications. (PDF)

S2 Fig. Δ-cyc expression in Pdf+ cells prevents sLN_vs fasciculation. (A) Representative timeline of the experiments in the figure. Flies were kept in LD conditions at 28°C for their entire lifespan. Dissections were performed within days 6-8 post-eclosion at ZT2-3. (B) Representative brain confocal images of anti-PDF (green) and anti-RFP (magenta) staining in the sLN_vs of flies in which Δ -cyc was constitutively expressed in the Pdf+ cells using a Pdf-Gal4;tub-Gal80^{ts} driver. Each line also included a Pdf-RFP transgene. White arrows indicate branching of sLN_v dorsal projections (left), and dorsal termini of the sLN_v projections (right) for the experimental genotype. The images are representative of two independent experiments. Scale bar = $50 \mu m$. LN_v morphology was quantified by comparing the sLN_v projection length until the branching point (C), the total number of intersections of the sLN_v ventral projections (D), the full sLN_v projection length (E), and the total number of lLN_v intersections (F). One-way ANOVA was used to analyze normally distributed data (C, F). For nonparametric data sets, a Kruskal-Wallis tests followed by Dunn's multiple comparisons tests was used (D,E). * p < 0.05, ** p < 0.01, *** p < 0.001. Error bars indicate SEM. Each dot corresponds to one brain. For each genotype: $9 \le n \le 12$. (G-H) Behavioral phenotypes of constitutive Δ -cyc expression. Experiments were conducted at 28°C. (G) Population Activity (left) plots for flies during days 3-5 of the LD cycle at 28°C (see Table 1 for additional quantifications). (H) Percent rhythmicity for the indicated genotypes under DD. R = Rhythmic and AR = arrhythmic. Fisher's exact contingency tests were used to analyze the percentage of rhythmic flies under DD (DD1-8). *** p < 0.001. Error bars indicate SEM. For each genotype: $24 \le n \le 32$. (PDF)

S3 Fig. Adult-specific *cyc* **knockdown does not affect sLNv neuronal morphology.** (A) Representative timeline of the experiments in the figure. Flies were raised in LD at 18°C, and

transferred to 28°C immediately after eclosion. Dissections were then performed within days 6-8 post-eclosion at ZT2-3. (B) Representative confocal images of anti-PDF (green) and anti-RFP (magenta) staining in the sLN_vs when cyc was downregulated exclusively after eclosion using a Pdf-Gal4;tub-Gal80^{ts} driver. The images are representative of two independent experiments. Scale bar = 50 μm. Each line also included a Pdf-RFP transgene. Kruskal-Wallis tests followed by Dunn's multiple comparisons tests were used to quantify the projection length until BP (C), the total number of intersections of the sLN_v ventral projections (D), the full sLN_v projection length (E), and the total number of lLN_v intersections (F). * p < 0.05. Datasets are nonparametric (C-F). Each dot corresponds to one brain. For each genotype: $17 \le n \le 24$. (G-H) Behavioral phenotypes of adult-specific cyc knockdown. Flies were raised in LD at 18°C, before being transferred to 28°C upon eclosion. Experiments were conducted at 28°C. (G) Population Activity plots for flies during days 3–5 of the LD cycle at 18°C (see Table 1 for additional quantifications). (H) Percent rhythmicity for the indicated genotypes under DD. Fisher's exact contingency tests were used to analyze the percentage of rhythmic flies under DD (DD1-8). *** p < 0.001. Error bars indicate SEM. For each genotype: $25 \le n \le 31$. (PDF)

S4 Fig. Expressing Δ -Clk in the LN_vs results in morphology and behavioral phenotypes. (A) Representative timeline. Flies were raised in LD at 28°C for their entire lifespan. Behavioral assays and dissections were performed within days 6-8 post-eclosion at ZT2-3. Experiments were conducted at 28°C. (B) Fisher's tests were used to compare the percent of rhythmic flies of each indicated genotype (additional quantifications can be found in Table 1). ** P < 0.01, *** P < 0.001. For each genotype: $21 \le n \le 26$. (C-D) Additional quantifications of effects of Clk^{RNAi} expression in the Pdf+ cells in adult brains. Neither the sLN_v total projection length (C) nor the lLN_v projections (D) were affected. Datasets were quantified with ordinary oneway ANOVA tests followed by Tukey's Multiple Comparisons tests. For each genotype: $16 \le n$ ≤ 22. (E) Fisher's tests were used to compare the percent of rhythmic flies of each indicated genotype (additional quantifications shown in Table 1). For each genotype: $27 \le n \le 31$. (F-G) Effects of Δ -Clk expression in the Pdf+ cells in adult brains. The sLN_v total projection length (F) and the lLN_v projections (G) were quantified using one-way ANOVA tests followed by Tukey's Multiple Comparisons tests. Each dot corresponds to one brain. For each genotype: 17 < n < 22. (H-J) Mann-Whitney tests were used to compare nuclear PER intensity levels in the sLN_vs (H), lLN_vs (J), and LN_ds (J) in flies of the indicated genotypes. Flies were raised at constant 28°C for their entire lifespan and dissections were performed at ZT2-3 * p < 0.05, ** P < 0.01, *** P < 0.001. Error bars indicate SEM. (PDF)

S5 Fig. Clk downregulation in the larval sLN_vs did not result in morphology phenotypes.

(A) Representative timeline of the experiments in the figure. Larvae were raised in LD at 28 °C. Third instar larvae (L3) were dissected at ZT2-3. (B) Representative confocal images of anti-RFP (magenta) staining in the sLN_vs when Clk^{RNAi} was expressed in L3 larvae. Each line also contains a Pdf-RFP transgene. Scale bar = 25 μ m. Kruskal-Wallis tests followed by Dunn's multiple comparisons tests were used to compare the projection length from the POI to the BP (C), the total number of axonal intersections (D), and the total projection length from the POI (E). * p < 0.05. Error bars indicate SEM. Each dot corresponds to one brain. For each genotype: $4 \le n \le 9$. (PDF)

S1 Table. Statistical Analysis for all Experiments. Statistical analysis of each experiment, labelled with the corresponding figure, the genotypes used, and the comparisons between

genotypes. D'Agostino & Pearson Normality tests were employed to determine if datasets followed a normal distribution. For comparisons between two independent variables unpaired ttests were used for parametric datasets, while Mann-Whitney tests were employed for nonparametric datasets. For comparisons between three independent variables ordinary one-way ANOVA tests followed by Tukey's Multiple Comparisons tests or Holm-Šídák's Multiple Comparisons tests were used for parametric datasets, while Kruskal-Wallis tests followed by Dunn's multiple comparisons tests were employed for nonparametric datasets. The p value for each test run is indicated, as is each tests corresponding significance. NS indicates results that are not significant. * p < 0.05, ** p < 0.01, *** p < 0.001. (XLSX)

Acknowledgments

We are very grateful to Justin Blau and Paul Hardin for their valuable feedback on various aspects of this project and for sharing fly lines with us. We are also grateful to M.Fernanda Ceriani, Amanda González-Segarra, Aishwarya Ramakrishnan Iyer, Orie Shafer, and Troy Shirangi for helpful comments on the manuscript, Annika Barber and Troy Shirangi for helpful discussions, Orie Shafer for the rat anti-PER antibody and Michael Rosbash for fly lines. The mouse anti-PDF antibody was obtained from the Developmental Studies Hybridoma Bank, created by the NICHD of the NIH and maintained at The University of Iowa, Department of Biology, Iowa City, IA 52242. Stocks obtained from the Bloomington *Drosophila* Stock Center (NIH P40OD018537) were used in this study.

Author Contributions

Conceptualization: Maria P. Fernandez.

Data curation: Grace Biondi.

Formal analysis: Grace Biondi, Gina McCormick, Maria P. Fernandez.

Funding acquisition: Maria P. Fernandez.

Investigation: Grace Biondi, Gina McCormick, Maria P. Fernandez.

Methodology: Grace Biondi, Maria P. Fernandez.

Project administration: Maria P. Fernandez.

Supervision: Maria P. Fernandez.

Visualization: Grace Biondi, Gina McCormick.

Writing - original draft: Maria P. Fernandez.

Writing - review & editing: Grace Biondi, Maria P. Fernandez.

References

- Herzog ED. Neurons and networks in daily rhythms. Nat Rev Neurosci. 2007; 8(10):790–802. Epub 2007/09/21. https://doi.org/10.1038/nrn2215 PMID: 17882255.
- Taghert PH, Nitabach MN. Peptide neuromodulation in invertebrate model systems. Neuron. 2012; 76
 (1):82–97. Epub 2012/10/09. https://doi.org/10.1016/j.neuron.2012.08.035 PMID: 23040808; PubMed Central PMCID: PMC3466441.
- Sehgal A, Price J, Young MW. Ontogeny of a biological clock in Drosophila melanogaster. Proc Natl Acad Sci U S A. 1992; 89(4):1423–7. Epub 1992/02/15. https://doi.org/10.1073/pnas.89.4.1423 PMID: 1741397; PubMed Central PMCID: PMC48463.

- Helfrich-Forster C. The neuroarchitecture of the circadian clock in the brain of Drosophila melanogaster. Microsc Res Tech. 2003; 62(2):94–102. Epub 2003/09/11. https://doi.org/10.1002/jemt.10357 PMID: 12966496.
- Shafer OT, Helfrich-Forster C, Renn SC, Taghert PH. Reevaluation of Drosophila melanogaster's neuronal circadian pacemakers reveals new neuronal classes. J Comp Neurol. 2006; 498(2):180–93. Epub 2006/07/21. https://doi.org/10.1002/cne.21021 PMID: 16856134; PubMed Central PMCID: PMC2596765.
- Schubert FK, Hagedorn N, Yoshii T, Helfrich-Forster C, Rieger D. Neuroanatomical details of the lateral neurons of Drosophila melanogaster support their functional role in the circadian system. J Comp Neurol. 2018; 526(7):1209–31. Epub 2018/02/10. https://doi.org/10.1002/cne.24406 PMID: 29424420; PubMed Central PMCID: PMC5873451.
- Hardin PE, Hall JC, Rosbash M. Feedback of the Drosophila period gene product on circadian cycling of its messenger RNA levels. Nature. 1990; 343(6258):536–40. Epub 1990/02/08. https://doi.org/10.1038/343536a0 PMID: 2105471.
- Cyran SA, Buchsbaum AM, Reddy KL, Lin MC, Glossop NR, Hardin PE, et al. vrille, Pdp1, and dClock form a second feedback loop in the Drosophila circadian clock. Cell. 2003; 112(3):329–41. Epub 2003/ 02/13. https://doi.org/10.1016/s0092-8674(03)00074-6 PMID: 12581523.
- Glossop NRJ, Houl JH, Zheng H, Ng FS, Dudek SM, Hardin PE. VRILLE Feeds Back to Control Circadian Transcription of Clock in the Drosophila Circadian Oscillator. Neuron. 2003; 37(2):249–61. https://doi.org/10.1016/s0896-6273(03)00002-3 PMID: 12546820
- Liu T, Mahesh G, Houl JH, Hardin PE. Circadian Activators Are Expressed Days before They Initiate Clock Function in Late Pacemaker Neurons from Drosophila. The Journal of Neuroscience. 2015; 35 (22):8662–71. https://doi.org/10.1523/JNEUROSCI.0250-15.2015 PMID: 26041931
- Ma D, Przybylski D, Abruzzi KC, Schlichting M, Li Q, Long X, et al. A transcriptomic taxonomy of Drosophila circadian neurons around the clock. eLife. 2021; 10:e63056. https://doi.org/10.7554/eLife.63056 PMID: 33438579
- Shafer OT, Gutierrez GJ, Li K, Mildenhall A, Spira D, Marty J, et al. Connectomic analysis of the Drosophila lateral neuron clock cells reveals the synaptic basis of functional pacemaker classes. Elife. 2022;11. Epub 2022/06/30. https://doi.org/10.7554/eLife.79139 PMID: 35766361; PubMed Central PMCID: PMC9365390.
- **13.** Helfrich-Forster C. Neurobiology of the fruit fly's circadian clock. Genes Brain Behav. 2005; 4(2):65–76. Epub 2005/02/22. https://doi.org/10.1111/j.1601-183X.2004.00092.x PMID: 15720403.
- Abruzzi KC, Zadina A, Luo W, Wiyanto E, Rahman R, Guo F, et al. RNA-seq analysis of Drosophila clock and non-clock neurons reveals neuron-specific cycling and novel candidate neuropeptides. PLoS Genet. 2017; 13(2):e1006613. Epub 2017/02/10. https://doi.org/10.1371/journal.pgen.1006613 PMID: 28182648; PubMed Central PMCID: PMC5325595.
- Rieger D, Shafer OT, Tomioka K, Helfrich-Forster C. Functional analysis of circadian pacemaker neurons in Drosophila melanogaster. J Neurosci. 2006; 26(9):2531–43. Epub 2006/03/03. https://doi.org/10.1523/JNEUROSCI.1234-05.2006 PMID: 16510731.
- Murad A, Emery-Le M, Emery P. A subset of dorsal neurons modulates circadian behavior and light responses in Drosophila. Neuron. 2007; 53(5):689–701. Epub 2007/03/03. https://doi.org/10.1016/j. neuron.2007.01.034 PMID: 17329209; PubMed Central PMCID: PMC1852515.
- Grima B, Chelot E, Xia R, Rouyer F. Morning and evening peaks of activity rely on different clock neurons of the Drosophila brain. Nature. 2004; 431(7010):869–73. Epub 2004/10/16. https://doi.org/10.1038/nature02935 PMID: 15483616.
- Stoleru D, Peng Y, Agosto J, Rosbash M. Coupled oscillators control morning and evening locomotor behaviour of Drosophila. Nature. 2004; 431(7010):862–8. Epub 2004/10/16. https://doi.org/10.1038/nature02926 PMID: 15483615.
- Ewer J, Frisch B, Hamblen-Coyle MJ, Rosbash M, Hall JC. Expression of the period clock gene within different cell types in the brain of Drosophila adults and mosaic analysis of these cells' influence on circadian behavioral rhythms. J Neurosci. 1992; 12(9):3321–49. Epub 1992/09/01. https://doi.org/10. 1523/JNEUROSCI.12-09-03321.1992 PMID: 1382123.
- Frisch B, Hardin PE, Hamblen-Coyle MJ, Rosbash M, Hall JC. A promoterless period gene mediates behavioral rhythmicity and cyclical per expression in a restricted subset of the Drosophila nervous system. Neuron. 1994; 12(3):555–70. Epub 1994/03/01. https://doi.org/10.1016/0896-6273(94)90212-7 PMID: 8155319.
- 21. Renn SC, Park JH, Rosbash M, Hall JC, Taghert PH. A pdf neuropeptide gene mutation and ablation of PDF neurons each cause severe abnormalities of behavioral circadian rhythms in Drosophila. Cell. 1999; 99(7):791–802. Epub 2000/01/05. https://doi.org/10.1016/s0092-8674(00)81676-1 PMID: 10619432.

- Shafer OT, Yao Z. Pigment-Dispersing Factor Signaling and Circadian Rhythms in Insect Locomotor Activity. Curr Opin Insect Sci. 2014; 1:73–80. Epub 2014/11/12. https://doi.org/10.1016/j.cois.2014.05. 002 PMID: 25386391; PubMed Central PMCID: PMC4224320.
- 23. Park JH, Helfrich-Forster C, Lee G, Liu L, Rosbash M, Hall JC. Differential regulation of circadian pace-maker output by separate clock genes in Drosophila. Proc Natl Acad Sci U S A. 2000; 97(7):3608–13. Epub 2000/03/22. https://doi.org/10.1073/pnas.97.7.3608 PMID: 10725392; PubMed Central PMCID: PMC16287.
- Klose MK, Bruchez MP, Deitcher DL, Levitan ES. Temporally and spatially partitioned neuropeptide release from individual clock neurons. Proc Natl Acad Sci U S A. 2021; 118(17). Epub 2021/04/21. https://doi.org/10.1073/pnas.2101818118 PMID: 33875606; PubMed Central PMCID: PMC8092580.
- Helfrich-Forster C, Shafer OT, Wulbeck C, Grieshaber E, Rieger D, Taghert P. Development and morphology of the clock-gene-expressing lateral neurons of Drosophila melanogaster. J Comp Neurol. 2007; 500(1):47–70. Epub 2006/11/14. https://doi.org/10.1002/cne.21146 PMID: 17099895.
- 26. Helfrich-Forster C, Homberg U. Pigment-dispersing hormone-immunoreactive neurons in the nervous system of wild-type Drosophila melanogaster and of several mutants with altered circadian rhythmicity. J Comp Neurol. 1993; 337(2):177–90. Epub 1993/11/08. https://doi.org/10.1002/cne.903370202 PMID: 8276996.
- Fernandez MP, Berni J, Ceriani MF. Circadian remodeling of neuronal circuits involved in rhythmic behavior. PLoS Biol. 2008; 6(3):e69. Epub 2008/03/28. https://doi.org/10.1371/journal.pbio.0060069
 PMID: 18366255: PubMed Central PMCID: PMC2270325.
- 28. Petsakou A, Sapsis Themistoklis P, Blau J. Circadian Rhythms in Rho1 Activity Regulate Neuronal Plasticity and Network Hierarchy. Cell. 2015; 162(4):823–35. https://doi.org/10.1016/j.cell.2015.07.010 PMID: 26234154
- 29. Gorostiza EA, Depetris-Chauvin A, Frenkel L, Pírez N, Ceriani María F. Circadian Pacemaker Neurons Change Synaptic Contacts across the Day. Current Biology. 2014; 24(18):2161–7. https://doi.org/10.1016/j.cub.2014.07.063 PMID: 25155512
- 30. Herrero A, Duhart JM, Ceriani MF. Neuronal and Glial Clocks Underlying Structural Remodeling of Pacemaker Neurons in Drosophila. Front Physiol. 2017; 8:918. Epub 2017/12/01. https://doi.org/10. 3389/fphys.2017.00918 PMID: 29184510; PubMed Central PMCID: PMC5694478.
- Depetris-Chauvin A, Fernández-Gamba Á, Gorostiza EA, Herrero A, Castaño EM, Ceriani MF. Mmp1 Processing of the PDF Neuropeptide Regulates Circadian Structural Plasticity of Pacemaker Neurons. PLOS Genetics. 2014; 10(10):e1004700. https://doi.org/10.1371/journal.pgen.1004700 PMID: 25356918
- Blau J, Young MW. Cycling vrille Expression Is Required for a Functional Drosophila Clock. Cell. 1999; 99(6):661–71. https://doi.org/10.1016/s0092-8674(00)81554-8 PMID: 10612401
- 33. Rutila JE, Suri V, Le M, So WV, Rosbash M, Hall JC. CYCLE is a second bHLH-PAS clock protein essential for circadian rhythmicity and transcription of Drosophila period and timeless. Cell. 1998; 93 (5):805–14. Epub 1998/06/18. https://doi.org/10.1016/s0092-8674(00)81441-5 PMID: 9630224.
- 34. Dong Z, Zhang G, Qu M, Gimple RC, Wu Q, Qiu Z, et al. Targeting Glioblastoma Stem Cells through Disruption of the Circadian Clock. Cancer Discov. 2019; 9(11):1556–73. Epub 2019/08/29. https://doi.org/10.1158/2159-8290.CD-19-0215 PMID: 31455674; PubMed Central PMCID: PMC6983300.
- Wagner PM, Prucca CG, Velazquez FN, Sosa Alderete LG, Caputto BL, Guido ME. Temporal regulation of tumor growth in nocturnal mammals: In vivo studies and chemotherapeutical potential. FASEB J. 2021; 35(2):e21231. Epub 2021/01/12. https://doi.org/10.1096/fj.202001753R PMID: 33428275.
- 36. Kondratova AA, Dubrovsky YV, Antoch MP, Kondratov RV. Circadian clock proteins control adaptation to novel environment and memory formation. Aging (Albany NY). 2010; 2(5):285–97. Epub 2010/06/04. https://doi.org/10.18632/aging.100142 PMID: 20519775; PubMed Central PMCID: PMC2898019.
- Kondratov RV, Kondratova AA, Gorbacheva VY, Vykhovanets OV, Antoch MP. Early aging and agerelated pathologies in mice deficient in BMAL1, the core component of the circadian clock. Genes Dev. 2006; 20(14):1868–73. Epub 2006/07/19. https://doi.org/10.1101/gad.1432206 PMID: 16847346; PubMed Central PMCID: PMC1522083.
- Zheng Y, Pan L, Wang F, Yan J, Wang T, Xia Y, et al. Neural function of Bmal1: an overview. Cell & Bioscience. 2023; 13(1):1. https://doi.org/10.1186/s13578-022-00947-8 PMID: 36593479
- Gunawardhana KL, Hardin PE. VRILLE Controls PDF Neuropeptide Accumulation and Arborization Rhythms in Small Ventrolateral Neurons to Drive Rhythmic Behavior in Drosophila. Curr Biol. 2017; 27 (22):3442–53 e4. Epub 2017/11/07. https://doi.org/10.1016/j.cub.2017.10.010 PMID: 29103936.
- 40. Goda T, Mirowska K, Currie J, Kim MH, Rao NV, Bonilla G, et al. Adult circadian behavior in Drosophila requires developmental expression of cycle, but not period. PLoS Genet. 2011; 7(7):e1002167. Epub 20110707. https://doi.org/10.1371/journal.pgen.1002167 PMID: 21750685; PubMed Central PMCID: PMC3131292.

- Ruben M, Drapeau MD, Mizrak D, Blau J. A mechanism for circadian control of pacemaker neuron excitability. J Biol Rhythms. 2012; 27(5):353–64. https://doi.org/10.1177/0748730412455918 PMID: 23010658; PubMed Central PMCID: PMC4019749.
- **42.** Sholl DA. Dendritic organization in the neurons of the visual and motor cortices of the cat. J Anat. 1953; 87(4):387–406. PMID: 13117757; PubMed Central PMCID: PMC1244622.
- Tanoue S, Krishnan P, Krishnan B, Dryer SE, Hardin PE. Circadian clocks in antennal neurons are necessary and sufficient for olfaction rhythms in Drosophila. Curr Biol. 2004; 14(8):638–49. https://doi.org/10.1016/j.cub.2004.04.009 PMID: 15084278.
- Collins B, Kane Elizabeth A, Reeves David C, Akabas Myles H, Blau J. Balance of Activity between LNvs and Glutamatergic Dorsal Clock Neurons Promotes Robust Circadian Rhythms in Drosophila. Neuron. 2012; 74(4):706–18. https://doi.org/10.1016/j.neuron.2012.02.034 PMID: 22632728
- 45. Lorber C, Leleux S, Stanewsky R, Lamaze A. Light triggers a network switch between circadian morning and evening oscillators controlling behaviour during daily temperature cycles. PLOS Genetics. 2022; 18 (11):e1010487. https://doi.org/10.1371/journal.pgen.1010487 PMID: 36367867
- 46. Siwicki KK, Eastman C, Petersen G, Rosbash M, Hall JC. Antibodies to the period gene product of Drosophila reveal diverse tissue distribution and rhythmic changes in the visual system. Neuron. 1988; 1 (2):141–50. Epub 1988/04/01. https://doi.org/10.1016/0896-6273(88)90198-5 PMID: 3152288.
- **47.** Hendricks JC, Lu S, Kume K, Yin JC, Yang Z, Sehgal A. Gender dimorphism in the role of cycle (BMAL1) in rest, rest regulation, and longevity in Drosophila melanogaster. J Biol Rhythms. 2003; 18 (1):12–25. Epub 2003/02/06. https://doi.org/10.1177/0748730402239673 PMID: 12568241.
- 48. McGuire SE, Mao Z, Davis RL. Spatiotemporal gene expression targeting with the TARGET and gene-switch systems in Drosophila. Sci STKE. 2004; 2004(220):pl6. Epub 2004/02/19. https://doi.org/10. 1126/stke.2202004pl6 PMID: 14970377.
- Mazzoni EO, Desplan C, Blau J. Circadian pacemaker neurons transmit and modulate visual information to control a rapid behavioral response. Neuron. 2005; 45(2):293–300. Epub 2005/01/25. https://doi.org/10.1016/j.neuron.2004.12.038 PMID: 15664180.
- Larderet I, Fritsch PMJ, Gendre N, Neagu-Maier GL, Fetter RD, Schneider-Mizell CM, et al. Organization of the Drosophila larval visual circuit. eLife. 2017; 6:e28387. https://doi.org/10.7554/eLife.28387
 PMID: 30726702
- Keene AC, Duboue ER, McDonald DM, Dus M, Suh GS, Waddell S, et al. Clock and cycle limit starvation-induced sleep loss in Drosophila. Curr Biol. 2010; 20(13):1209–15. Epub 2010/06/15. https://doi.org/10.1016/j.cub.2010.05.029 PMID: 20541409; PubMed Central PMCID: PMC2929698.
- 52. Sivachenko A, Li Y, Abruzzi KC, Rosbash M. The transcription factor Mef2 links the Drosophila core clock to Fas2, neuronal morphology, and circadian behavior. Neuron. 2013; 79(2):281–92. Epub 2013/07/31. https://doi.org/10.1016/j.neuron.2013.05.015 PMID: 23889933; PubMed Central PMCID: PMC3859024.
- 53. Richhariya S, Shin D, Le JQ, Rosbash M. Dissecting neuron-specific functions of circadian genes using modified cell-specific CRISPR approaches. Proc Natl Acad Sci U S A. 2023; 120(29):e2303779120. Epub 2023/07/10. https://doi.org/10.1073/pnas.2303779120 PMID: 37428902; PubMed Central PMCID: PMC10629539.
- 54. Houl JH, Ng F, Taylor P, Hardin PE. CLOCK expression identifies developing circadian oscillator neurons in the brains of Drosophila embryos. BMC Neurosci. 2008; 9:119. Epub 20081218. https://doi.org/10.1186/1471-2202-9-119 PMID: 19094242; PubMed Central PMCID: PMC2628352.
- 55. Herrero A, Yoshii T, Ispizua JI, Colque C, Veenstra JA, Muraro NI, et al. Coupling Neuropeptide Levels to Structural Plasticity in Drosophila Clock Neurons. Curr Biol. 2020; 30(16):3154–66 e4. Epub 2020/07/04. https://doi.org/10.1016/j.cub.2020.06.009 PMID: 32619484.
- Miller CM, Page-McCaw A, Broihier HT. Matrix metalloproteinases promote motor axon fasciculation in the Drosophila embryo. Development. 2008; 135(1):95–109. Epub 2007/11/30. https://doi.org/10.1242/dev.011072 PMID: 18045838.
- 57. Gorostiza EA, Ceriani MF. Retrograde Bone Morphogenetic Protein Signaling Shapes a Key Circadian Pacemaker Circuit. The Journal of Neuroscience. 2013; 33(2):687–96. https://doi.org/10.1523/ JNEUROSCI.3448-12.2013 PMID: 23303947
- Das P, L. Maduzia L, Wang H, L.Finelli A, Cho S-H Smith MM, et al. The Drosophila gene Medea demonstrates the requirement for different classes of Smads in dpp signaling. Development. 1998; 125 (8):1519–28. https://doi.org/10.1242/dev.125.8.1519 PMID: 9502733
- Zhao J, Kilman VL, Keegan KP, Peng Y, Emery P, Rosbash M, et al. Drosophila clock can generate ectopic circadian clocks. Cell. 2003; 113(6):755–66. Epub 2003/06/18. https://doi.org/10.1016/s0092-8674(03)00400-8 PMID: 12809606.

- 60. Liu T, Mahesh G, Yu W, Hardin PE. CLOCK stabilizes CYCLE to initiate clock function in Drosophila. Proc Natl Acad Sci U S A. 2017; 114(41):10972–7. Epub 2017/10/05. https://doi.org/10.1073/pnas. 1707143114 PMID: 28973907; PubMed Central PMCID: PMC5642697.
- 61. Kula-Eversole E, Nagoshi E, Shang Y, Rodriguez J, Allada R, Rosbash M. Surprising gene expression patterns within and between PDF-containing circadian neurons in Drosophila. Proc Natl Acad Sci U S A. 2010; 107(30):13497–502. Epub 2010/07/14. https://doi.org/10.1073/pnas.1002081107 PMID: 20624977; PubMed Central PMCID: PMC2922133.
- Patop IL, Anduaga AM, Bussi IL, Ceriani MF, Kadener S. Organismal landscape of clock cells and circadian gene expression in Drosophila. bioRxiv. 2023:2023.05.23.542009. https://doi.org/10.1101/2023.05.23.542009 PMID: 37292867
- Reick M, Garcia JA, Dudley C, McKnight SL. NPAS2: An Analog of Clock Operative in the Mammalian Forebrain. Science. 2001; 293(5529):506–9. https://doi.org/10.1126/science.1060699 PMID: 11441147
- 64. Shokri L, Inukai S, Hafner A, Weinand K, Hens K, Vedenko A, et al. A Comprehensive Drosophila melanogaster Transcription Factor Interactome. Cell Rep. 2019; 27(3):955–70.e7. Epub 2019/04/18. https://doi.org/10.1016/j.celrep.2019.03.071 PMID: 30995488; PubMed Central PMCID: PMC6485956.
- 65. Fernandez MP, Pettibone HL, Bogart JT, Roell CJ, Davey CE, Pranevicius A, et al. Sites of Circadian Clock Neuron Plasticity Mediate Sensory Integration and Entrainment. Curr Biol. 2020; 30(12):2225–37 e5. Epub 2020/05/11. https://doi.org/10.1016/j.cub.2020.04.025 PMID: 32386535; PubMed Central PMCID: PMC7314648.